American Mineralogist, Volume 84, pages 650–664, 1999

The Gibbs free energies and enthalpies of formation of U^{6+} phases: An empirical method of prediction

FANRONG CHEN,[1,*] RODNEY C. EWING,[1,2,†] AND SUE B. CLARK[3]

[1]Department of Nuclear Engineering and Radiological Sciences, University of Michigan, Ann Arbor, Michigan 48109-2104, U.S.A.
[2]Department of Geological Sciences, University of Michigan, Ann Arbor, Michigan 48109-1063, U.S.A.
[3]Department of Chemistry, Washington State University, Pullman, Washington 99164, U.S.A.

ABSTRACT

Uranyl minerals form as a result of the oxidation and alteration of uraninite, UO_{2+x}. These uranyl phases are also important alteration products of the corrosion of UO_2 in used nuclear fuels under oxidizing conditions. However, the thermodynamic database for these phases is extremely limited. The Gibbs free energies and enthalpies for uranyl phases are estimated based on a method that sums polyhedral contributions. The molar contributions of the structural components to ΔG_f^0 and ΔH_f^0 are derived by multiple regression using the thermodynamic data of phases for which the crystal structures are known. In comparison with experimentally determined values, the average residuals associated with the predicted ΔG_f^0 and ΔH_f^0 for the uranyl phases used in the model are 0.08 and 0.10%, respectively, well below the limits of uncertainty for the experimentally determined values. To analyze the reliability of the predicted ΔG_f^0 values, activity-activity diagrams in SiO_2-CaO-UO_3-H_2O and CO_2-CaO-UO_3-H_2O systems at 298.15 K and 1 bar were constructed using the predicted $\Delta G_{f,298.15}^0$ values for the relevant U^{6+} phases. There is good agreement between the predicted mineral stability relations and field occurrences, thus providing confidence in this method for the estimation of ΔG_f^0 and ΔH_f^0 of the U^{6+} phases.

INTRODUCTION

UO_2 under oxidizing conditions is not stable and rapidly forms a wide variety of uranyl oxyhydroxides, silicates, phosphates, carbonates, and vanadates depending on groundwater compositions (Langmuir 1978; Finch and Ewing 1992). The paragenesis and stability of these phases have long been of interest with many studies emphasizing the role of oxidation and reduction reactions in the formation of uranium deposits (McKelvey et al. 1955; Garrels and Christ 1959; Garrels and Weeks 1959). However, there has been renewed interest in these phases because they form as alteration products in uranium tailings and on used nuclear fuel under oxidizing conditions (Wronkiewicz et al. 1992). The nuclear fuel consists predominantly of UO_2, but fission and neutron-capture reactions result in approximately 4% fission products and actinides after a burnup of 40 MWd/kgU (Barner 1985; Johnson and Shoesmith 1988; Johnson and Werme 1994; Oversby 1994). In the presence of an oxidizing aqueous phase, especially involving radiolytically produced oxidants, the alteration rate of spent fuel is appreciable (Shoesmith and Sunder 1992; Sunder et al. 1998). A critical issue is the fate of the released radionuclides during the alteration and matrix corrosion of the UO_2. Some of the radionuclides are incorporated into the secondary uranyl phases (Frondel 1958; Finch and Ewing 1991, 1992; Burns et al. 1997a, 1997c) and, in fact, these phases may become the primary source term for the release of radionuclides. Thus, the paragenesis, structures, and stabilities of these phases are of critical importance in evaluating the long-term behavior of spent nuclear fuel in a repository under oxidizing conditions.

Unfortunately, the thermodynamic database for these uranyl phases is limited and in some cases contradictory (Grenthe et al. 1992). There is an immediate need to be able to estimate thermodynamic parameters and solubility constants. This paper represents an effort to estimate by regression analysis the standard Gibbs free energies (ΔG_f^0) and enthalpies (ΔH_f^0) of formation of U^{6+} phases based on their structural components. Although the present experimental data are limited and the different types of uranyl polyhedra were not treated separately in this analysis, this approach allows one to utilize all data presently available and will allow for the immediate refinement of estimated thermodynamic values as new experimental data become available. We also identify phases for which future structural analysis and additional thermodynamic data will provide the greatest impact on the development of the required database. Additionally, the estimated values may be used when suitable samples are not available for experimental determinations (i.e., uranyl phases that commonly occur as fine-grained mixtures of variable composition).

*Permanent address: Guangzhou Institute of Geochemistry, Chinese Academy of Sciences, Wushan, Guangzhou 510640, P.R. China.
†E-mail: rodewing@umich.edu

For silicate minerals, many approaches exist for estimating ΔG_f^0 (Karpov and Kashik 1968; Chen 1975; Nriagu 1975; Tardy and Garrels 1974, 1976, 1977; Mattigod and Sposito 1978; Sposito 1986) and ΔH_f^0 (Hemingway et al. 1982; Vieillard and Tardy 1988). Most of these methods are based on the observation that the ΔG_f^0 and ΔH_f^0 of minerals can be estimated by summing, in stoichiometric proportions, the contributions of simpler constituent components. Because the contributions of the oxide and hydroxides to ΔG_f^0 and ΔH_f^0 largely depend on the coordination numbers of the cations involved, the oxide or hydroxide of the same cation with different coordination number should be treated differently. In this study, the ΔG_f^0 and ΔH_f^0 of U^{6+} minerals are considered to be the sum of oxide polyhedral contributions that were determined by multiple linear regression. This method is similar to that developed by Chermak and Rimstidt (1989) for estimating the ΔG_f^0 and ΔH_f^0 of silicate minerals.

PREVIOUS WORK

The empirical method developed by Chen (1975) was adopted by Hemingway (1982) to estimate the ΔG_f^0 of uranyl silicates. For silicate minerals, the error of estimation made by this method is, in most cases, <0.6% and seems slightly larger for uranyl silicates. Van Genderen and Van Der Weijden (1984) applied the method developed by Tardy and Garrels (1976) to uranyl phases. It is based upon the linear relationship between two parameters, ΔO and ΔF (ΔO is the difference of the Gibbs free energies of formation of the oxide and the aqueous cation for a specific element in the mineral; ΔF is the Gibbs free energy of the formation reaction of a mineral from the constituent oxides and the acids). This method is applicable only within a mineral group with the same structure (i.e., coordinations for all the cations are the same in the structure) because minor differences in the structure of the same mineral group can have appreciable influences on the empirical relationships between ΔO and ΔF. Considering the complexity of uranyl phases and the scarcity of reliable thermodynamic data for these phases, the application of this approach is limited.

Recent attempts to estimate ΔG_f^0 for U^{6+} minerals have been made by Finch (1997) and Clark et al. (1998). Both used a method similar to that developed by Tardy and Garrels (1974) for estimating the ΔG_f^0 for silicate minerals. This method is based on the assumption that a particular constituent oxide makes the same contribution to the ΔG_f^0 for all minerals considered; thus, the ΔG_f^0 of a mineral is the arithmetic sum of its constituent oxide contributions. The g_i of SiO_2, Na_2O, K_2O, CaO, and MgO given by Clark et al. (1998) were assumed to be equal to those in silicate structures and are taken directly from Tardy and Garrels (1974) and, thus, the predicted values of ΔG_f^0 for U^{6+} phases are significantly different from those obtained by experiment. [Note that g_i and h_i (see below) represent the molar Gibbs free energy and enthalpy, respectively, of the corresponding oxide.] Because there were no independent data for comparison to the estimated values, Finch (1997) constructed activity-activity diagrams for the SiO_2-CaO-UO_3-H_2O and CO_2-CaO-UO_3-H_2O systems using estimated ΔG_f^0 values. The stability relations among the relevant minerals illustrated by the diagrams were in qualitative agreement with geological observations for the occurrences of these minerals. However, because this method used the ΔG_f^0 of a specific mineral to derive the g_i of a constituent oxide (except UO_3 and H_2O), the errors in the ΔG_f^0 values propagate through the derived g_i, and the g_i derived in this way depends, partly, on the selected ΔG_f^0 and the sequence by which each g_i is derived.

In addition, hexavalent uranium, U^{6+}, is almost always combined with two O atoms to form an independent UO_2^{2+} uranyl cation (Evans 1963). This approximately linear "dioxocation" is the only form of hexavalent uranium in solution (Baran 1992) and also predominates in solid phases (Burns et al. 1997b). In contrast to Si^{4+}, which almost always occupies tetrahedral sites in silicate structures, the uranyl cation is coordinated by four, five, or six anions in an approximately coplanar arrangement (Burns et al. 1996, 1997b) to form $Ur\phi_4$, $Ur\phi_5$, or $Ur\phi_6$ bipyramidal polyhedra (Ur: uranyl ion; ϕ: anion) with the oxygen atoms that are part of the uranyl ion located at the opposing apices. These uranyl polyhedra are proposed to be treated as different structural components in this paper. Moreover, molecular water and structural hydroxyl must be treated differently due to their distinctive structural functions. The previous methods did not consider the different coordinations of the cations and, thus, are best used within a group of structurally similar phases.

The approach proposed in this paper offers the following advantages over previous estimation techniques. (1) The structural component-summation technique provides smaller uncertainty relative to the oxide-summation technique if the coordination of the cation is considered. (2) The ΔG_f^0 and ΔH_f^0 may be estimated even though data for representative phases in similar structural classes are not available because each type of cation polyhedron is considered to possess a set of well-defined properties (Hazen 1985, 1988). (3) Small errors in individual data of the reference phases can be reduced through the averaging provided by multiple regression. Although different types of uranyl polyhedra were treated as a single structural component owing to the present limitations of the thermodynamic database, the predicted results using this approach are in better agreement with geological observations than those of previous studies and will facilitate further improvement as more accurately determined thermodynamic data for uranyl phases with uranium in different coordinations become available.

FICTIVE STRUCTURAL COMPONENTS

A fictive structural component is a cation coordination polyhedron with a similar structural function, and it may be expressed in the form of an oxide or hydroxide. Because the cations in crystal structures are commonly coordinated directly to O atoms, and the hydrogen ions sharing O with other cations are considered to be part of the structural water (see discussion below), all structural components are expressed as "cation oxides" in this study.

In U^{6+} phases, the basic fictive structural components are uranyl polyhedra with different coordination numbers (Burns et al. 1997b). One $Ur\phi_n$ polyhedron polymerizes with other $Ur\phi_n$ or other cation coordination polyhedra to form clusters, chains, sheets, and even framework structures (Burns et al. 1996). The structural units (clusters, chains, and sheets) are connected by hydrogen bonds and low-valence cations that are commonly

coordinated by 8–12 anions and are denoted by the subscript (I). In framework structures, the similar structural components are coordination polyhedra of those cations located in channels parallel to [001] in a perovskite-like structure (Burns et al. 1996) or in the voids of other structure types with coordination numbers of 8–12. The structural function of hydrogen ions that are part of the structural water is similar to that of low-valance cations in sharing O with cations in the structure units, compensating charge in the structure, and connecting the structural units. Thus, structural water [$H_2O_{(S)}$] is regarded as an individual structural component and is different from the water of hydration [$H_2O_{(H)}$].

On the other hand, the coordination polyhedra of cations other than UO_2^{2+} may also form an individual coordination polyhedron within the structural units. These cations are different from those located in inter-structural unit sites. Their coordination numbers are no more than six and are indicated by the Roman numeral in the subscript of the relevant structural components. Constituent fictive structural components of 99 U^{6+} phases are listed in Table 1, which includes all the uranyl phases that may be important during the alteration of uraninite and spent UO_2 fuel.

TABLE 1. Constituent structural components for selected U^{6+} phases

Mineral	Formula	Constituent structural components	Ref.
	α-$[(UO_2)(OH)_2]$	$H_2O_{(S)}$ + $Ur\phi_6$	1
	β-$[(UO_2)(OH)_2]$	$H_2O_{(S)}$ + $Ur\phi_4$	2
	γ-$[(UO_2)(OH)_2]$	$H_2O_{(S)}$ + $Ur\phi_4$	3
schoepite	$[(UO_2)_8O_2(OH)_{12}](H_2O)_{12}$	$6H_2O_{(S)}$ + $8Ur\phi_5$ + $12H_2O_{(H)}$	4
meta-schoepite	$[(UO_2)_8O_2(OH)_{12}](H_2O)_{10}$	$6H_2O_{(S)}$ + $8Ur\phi_5$ + $10H_2O_{(H)}$	5
	$[(UO_3)(H_2O)_{0.9}]$	$0.9H_2O_{(S)}$ + $Ur\phi_6$	6
	$Li_2[(UO_2)O_2]$	$Li_2O_{(I)}$ + $Ur\phi_4$	7
	$Li_4[(UO_2)O_3]$	$2Li_2O_{(I)}$ + $Ur\phi_4$	8
	β-$Na_2[(UO_2)O_2]$	$Na_2O_{(I)}$ + $Ur\phi_4$	9
	$Na_4[(UO_2)O_3]$	$2Na_2O_{(I)}$ + $Ur\phi_4$	10
	$Na_2U_2O_7$	$Na_2O_{(I)}$ + $2Ur\phi_6$	11
	K_2UO_4	$K_2O_{(I)}$ + $Ur\phi_4$	12
	$K_2[(UO_2)_2O_3]$	$K_2O_{(I)}$ + $Ur\phi_5$ + $Ur\phi_4$	13
	$K_2[(UO_2)_5O_8](UO_2)_2$	$K_2O_{(I)}$ + $6Ur\phi_5$ + $Ur\phi_4$	14
	Cs_2UO_4	$Cs_2O_{(I)}$ + $Ur\phi_4$	15
	$Cs_4U_5O_{17}$	$2Cs_2O_{(I)}$ + $Ur\phi_5$ + $4Ur\phi_4$	15
	Rb_2UO_4	$Rb_2O_{(I)}$ + $Ur\phi_4$	16
becquerelite	$Ca[(UO_2)_3O_2(OH)_3]_2(H_2O)_8$	$CaO_{(I)}$ + $3H_2O_{(S)}$ + $6Ur\phi_5$ + $8H_2O_{(H)}$	17
	$SrUO_4$	$SrO_{(I)}$ + $Ur\phi_4$	18
	$[Sr_3(UO_2)_{11}O_{14}]$	$3SrO_{(VII)}$ + $5Ur\phi_5$ + $6Ur\phi_4$	19
	$BaUO_4$	$BaO_{(I)}$ + $Ur\phi_4$	20
	BaU_2O_7	$BaO_{(I)}$ + $2Ur\phi_4$	21
	Ba_3UO_6	$2BaO_{(I)}$ + $BaO_{(VI)}$ + $Ur\phi_4$	18
	Ba_2MgUO_6	$2BaO_{(I)}$ + $MgO_{(VI)}$ + $Ur\phi_4$	18
	Ba_2CaUO_6	$2BaO_{(I)}$ + $CaO_{(VI)}$ + $Ur\phi_4$	18
	Ba_2SrUO_6	$2BaO_{(I)}$ + $SrO_{(VI)}$ + $Ur\phi_4$	18
protasite	$Ba[(UO_2)_3O_3(OH)_2](H_2O)_3$	$BaO_{(I)}$ + $H_2O_{(S)}$ + $3Ur\phi_5$ + $3H_2O_{(H)}$	17
billietite	$Ba[(UO_2)_3O_2(OH)_3]_2(H_2O)_4$	$BaO_{(I)}$ + $3H_2O_{(S)}$ + $6Ur\phi_5$ + $4H_2O_{(H)}$	17
	$MgUO_4$	$MgO_{(VI)}$ + $Ur\phi_4$	22
	$PbUO_4$	$PbO_{(I)}$ + $Ur\phi_4$	23
fourmarierite	$Pb[(UO_2)_4O_3(OH)_4](H_2O)_4$	$PbO_{(I)}$ + $2H_2O_{(S)}$ + $4Ur\phi_5$ + $4H_2O_{(H)}$	24
sayrite	$Pb_2[(UO_2)_5O_6(OH)_2](H_2O)_4$	$2PbO_{(I)}$ + $H_2O_{(S)}$ + $4Ur\phi_5$ + $Ur\phi_4$ + $4H_2O_{(H)}$	25
curite	$Pb_3[(UO_2)_8O_8(OH)_6](H_2O)_3$	$3PbO_{(I)}$ + $3H_2O_{(S)}$ + $6Ur\phi_5$ + $2Ur\phi_4$ + $3H_2O_{(H)}$	26
α-uranophane	$Ca[(UO_2)(SiO_3OH)]_2(H_2O)_5$	$CaO_{(I)}$ + $H_2O_{(S)}$ + $2Ur\phi_5$) + $2SiO_{2(IV)}$ + $5H_2O_{(H)}$	27
boltwoodite	$(K,Na)[(UO_2)(SiO_3OH)](H_2O)_{1.5}$	$0.5(K,Na)_2O_{(I)}$ + $0.5H_2O_{(S)}$ + $Ur\phi_5$ + $SiO_{2(IV)}$ + $1.5H_2O_{(H)}$	28
cupro-sklodowskite	$Cu[(UO_2)(SiO_3OH)]_2(H_2O)_6$	$CuO_{(I)}$ + $H_2O_{(S)}$ + $2Ur\phi_5$ + $2SiO_{2(IV)}$ + $6H_2O_{(H)}$	29
sklodowskite	$Mg[(UO_2)(SiO_3OH)]_2(H_2O)_6$	$MgO_{(I)}$ + $H_2O_{(S)}$ + $2Ur\phi_5$ + $2SiO_{2(IV)}$ + $6H_2O_{(H)}$	30
kasolite	$Pb[(UO_2)(SiO_4)](H_2O)$	$PbO_{(I)}$ + $Ur\phi_5$ + $SiO_{2(IV)}$ + $H_2O_{(H)}$	31
β-uranophane	$Ca[(UO_2)(SiO_3OH)]_2(H_2O)_5$	$CaO_{(I)}$ + $H_2O_{(S)}$ + $2Ur\phi_5$ + $2SiO_{2(IV)}$ + $5H_2O_{(H)}$	32
soddyite	$[(UO_2)_2(SiO_4)](H_2O)_2$	$2Ur\phi_5$ + $SiO_{2(IV)}$ + $2H_2O_{(S)}$	33
weeksite	$(Na,K)_2[(UO_2)_2(Si_5O_{13})](H_2O)_3$	$(Na,K)_2O_{(I)}$ + $2Ur\phi_5$ + $5SiO_{2(IV)}$ + $3H_2O_{(S)}$	34
chernikovite	$[(UO_2)H(PO_4)](H_2O)_4$	$0.5H_2O_{(S)}$ + $Ur\phi_4$) + $0.5P_2O_{5(IV)}$+$4H_2O_{(H)}$	35
phosphuranylite	$KCa(H_3O)(UO_2)[(UO_2)_3(PO_4)_2O_2](H_2O)_8$	$0.5K_2O_{(I)}$ + $CaO_{(I)}$ + $6H_2O(s)$ + $Ur\phi_4$ + $4Ur\phi_5$ + $8H_2O_{(H)}$	36
	$K[(UO_2)(PO_4)](D_2O)_3$	$0.5K_2O_{(I)}$ + $Ur\phi_4$ + $0.5P_2O_{5(IV)}$ + $3D_2O_{(H)}$	37
	$Cs[(UO_2)(PO_3)_3]$	$0.5Cs_2O_{(I)}$ + $Ur\phi_5$ + $1.5P_2O_{5(IV)}$	38
	$Na_2[(UO_2)(P_2O_7)]$	$Na_2O_{(I)}$ + $Ur\phi_5$ + $P_2O_{5(IV)}$	39
saleeite	$Mg[(UO_2)(PO_4)]_2(H_2O)_{10}$	$MgO_{(I)}$ + $2Ur\phi_4$ + $P_2O_{5(IV)}$ + $10H_2O_{(H)}$	40
meta-autunite	$Ca[(UO_2)(PO_4)]_2(H_2O)_6$	$CaO_{(I)}$ + $2Ur\phi_4$ + $P_2O_{5(IV)}$ + $6H_2O_{(H)}$	41
meta-uranocircite	$Ba[(UO_2)(PO_4)]_2(H_2O)_6$	$BaO_{(I)}$ + $2Ur\phi_4$ + $P_2O_{5(IV)}$ + $6H_2O_{(H)}$	42
	$Al[(UO_2)_3O(OH)(PO_4)_2]$ $(H_2O)_7$	$0.5Al_2O_{3(I)}$ + $0.5H_2O_{(S)}$ + $3Ur\phi_4$ + $P_2O_{5(IV)}$ + $7H_2O_{(H)}$	43
threadgoldite	$Al[(UO_2)(PO_4)]_2(OH)(H_2O)_8$	$0.5Al_2O_{3(I)}$ + $0.5H_2O_{(S)}$ + $2Ur\phi_4$ + $P_2O_{5(IV)}$ + $8H_2O_{(H)}$	44
	$K_4[(UO_2)(PO_4)_2]$	$2K_2O_{(I)}$ + $Ur\phi_4$ + $P_2O_{5(IV)}$	45
phurcalite	$Ca_2[(UO_2)_3(PO_4)O_2]\cdot 7H_2O$	$2CaO_{(I)}$ + $2Ur\phi_5$ + $Ur\phi_6$ + $P_2O_{5(IV)}$ + $7H_2O_{(H)}$	46
phuralumite	$Al_2[(UO_2)_3(PO_4)_2(OH)_2]$ $(OH)_4(H_2O)_{10}$	$Al_2O_{3(I)}$ + $3H_2O_{(S)}$ + $2Ur\phi_5$ + $Ur\phi_6$ + $P_2O_{5(IV)}$ + $10H_2O_{(H)}$	47
althupite	$AlThUO_2[(UO_2)_3(PO_4)_2O$ $(OH)]_2$ $(OH)_3(H_2O)_{15}$	$0.5Al_2O_{3(I)}$ + $ThO_{2(I)}$ + $2.5H_2O_{(S)}$ + $3Ur\phi_5$ + $Ur\phi_6$ + $P_2O_{5(IV)}$ + $15H_2O_{(H)}$	48
meta-torbernite	$Cu_{0.92}[(UO_2)(PO_4)]_2(H_2O)_8$	$0.92CuO_{(I)}$ + $2Ur\phi_4$ + $P_2O_{5(IV)}$ + $8H_2O_{(H)}$	49

TABLE 1 *Continued*

Mineral	Formula	Constituent structural components	Ref.
meta-zeunerite	$Cu[(UO_2)(AsO_4)]_2(H_2O)_8$	$CuO_{(I)} + 2Ur\phi_4 + As_2O_{5(IV)} + 8H_2O_{(H)}$	50
abernathyite	$K[(UO_2)(AsO_4)](H_2O)_3$	$0.5K_2O_{(I)} + Ur\phi_4 + 0.5As_2O_{5(IV)} + 3H_2O_{(H)}$	51
	$KH_3O[(UO_2)(AsO_4)]_2(H_2O)_6$	$1.5H_2O_{(S)} + 0.5K_2O_{(I)} + 2Ur\phi_4 + As_2O_{5(IV)} + 6H_2O_{(H)}$	52
	$(UO_2)(SO_4)(H_2O)_{3.5}$	$2H_2O_{(S)} + Ur\phi_5 + SO_{3(IV)} + 1.5H_2O_{(H)}$	53
	$(UO_2)(SO_4)(H_2O)_{2.5}$	$2H_2O_{(S)} + Ur\phi_5 + SO_{3(IV)} + 0.5H_2O_{(H)}$	53
	$[(UO_2)(SO_4)(H_2O)_2]_2(H_2O)_3$	$2H_2O_{(S)} + Ur\phi_5 + SO_{3(IV)} + H_2O_{(H)}$	54
	β–$(UO_2)(SO_4)$	$Ur\phi_5 + SO_{3(IV)}$	55
	$Cs_2[(UO_2)_2(SO_4)_3]$	$Cs_2O_{(I)} + 2Ur\phi_5 + 3SO_{3(IV)}$	56
	$Mg[(UO_2)(SO_4)_2](H_2O)_{11}$	$MgO_{(I)} + Ur\phi_5 + 2SO_{3(IV)} + 11H_2O_{(H)}$	57
	$[H_2(UO_2)(SO_4)_2](H_2O)_5$	$H_2O_{(S)} + Ur\phi_5 + 2SO_{3(IV)} + 5H_2O_{(H)}$	58
	$K_2[(UO_2)(SO_4)_2](H_2O)_2$	$K_2O_{(I)} + Ur\phi_5 + 2SO_{3(IV)} + 2H_2O_{(H)}$	59
zippeite	$K[(UO_2)_2(SO_4)(OH)_3](H_2O)$	$0.5K_2O_{(I)} + 1.5H_2O_{(S)} + 2Ur\phi_5 + SO_{3(IV)} + H_2O_{(H)}$	60
rutherfordine	$(UO_2)(CO_3)$	$Ur\phi_6 + CO_{2(III)}$	61
liebigite	$Ca_2[(UO_2)(CO_3)_3](H_2O)_{11}$	$2CaO_{(I)} + Ur\phi_6 + 3CO_{2(III)} + 11H_2O_{(H)}$	62
bayleyite	$Mg_2[(UO_2)(CO_3)_3](H_2O)_{18}$	$2MgO_{(I)} + Ur\phi_6 + 3CO_{2(III)} + 18H_2O_{(H)}$	63
swartzite	$CaMg[(UO_2)(CO_3)_3](H_2O)_{12}$	$CaO_{(I)} + MgO_{(I)} + Ur\phi_6 + 3CO_{2(III)} + 12H_2O_{(H)}$	64
andersonite	$Na_2Ca[(UO_2)(CO_3)_3](H_2O)_5$	$Na_2O_{(I)} + CaO_{(I)} + Ur\phi_6 + 3CO_{2(III)} + 5H_2O_{(H)}$	65
	$Cs_4[(UO_2)(CO_3)_3](H_2O)_6$	$2Cs_2O_{(I)} + Ur\phi_6 + 3CO_{2(III)} + 6H_2O_{(H)}$	66
	$Sr_2[(UO_2)(CO_3)_3](H_2O)_8$	$2SrO_{(I)} + Ur\phi_6 + 3CO_{2(III)} + 8H_2O_{(H)}$	67
	$Rb[(UO_2)(NO_3)_3]$	$0.5Rb_2O_{(I)} + Ur\phi_6 + 1.5N_2O_{5(III)}$	68
	$[(UO_2)(NO_3)_2](H_2O)_6$	$Ur\phi_6 + N_2O_{5(III)} + 6H_2O_{(H)}$	69
	$[(UO_2)(NO_3)_2(H_2O)_3$	$Ur\phi_6 + N_2O_{5(III)} + 3H_2O_{(H)}$	70
	$[(UO_2)(NO_3)_2](H_2O)_2$	$Ur\phi_6 + N_2O_{5(III)} + 2H_2O_{(H)}$	70
	$[(UO_2)_2(OH)_2(NO_3)_2](H_2O)_4$	$H_2O_{(S)} + Ur\phi_6 + Ur\phi_5 + N_2O_{5(III)} + 4H_2O_{(H)}$	71
	$[(UO_2)_3O(OH)_3(H_2O)_6](NO_3)(H_2O)_4$	$7.5H_2O_{(S)} + 3Ur\phi_5 + 0.5N_2O_{5(III)} + 4H_2O_{(H)}$	72
	$Na[(UO_2)(BO_3)]$	$0.5Na_2O_{(I)} + Ur\phi_5 + 0.5B_2O_{3(III)}$	73
	$Li[(UO_2)(BO_3)]$	$0.5Li_2O_{(I)} + Ur\phi_5 + 0.5B_2O_{3(III)}$	74
	$[Mg(UO_2)(B_2O_5)]$	$MgO_{(VI)} + Ur\phi_5 + B_2O_{3(III)}$	75
	$[Ca(UO_2)_2(BO_3)_2]$	$CaO_{(VII)} + Ur\phi_4 + Ur\phi_5 + B_2O_{3(III)}$	76
francevillite	$Ba_{0.96}Pb_{0.04}[(UO_2)_2(V_2O_8)](H_2O)_5$	$0.96BaO_{(I)} + 0.04PbO_{(I)} + {}_2Ur\phi_5 + V_2O_{5(V)} + 5H_2O_{(H)}$	77
	$Pb[(UO_2)_2(V_2O_8)](H_2O)_5$	$PbO_{(I)} + 2Ur\phi_5 + V_2O_{5(V)} + 5H_2O_{(H)}$	78
	$K_2[(UO_2)_2(V_2O_8)]$	$K_2O_{(I)} + 2Ur\phi_5 + V_2O_{5(V)}$	79
sengierite	$Cu_2[(UO_2)_2(V_2O_8)(OH)_2](H_2O)_6$	$2CuO_{(I)} + H_2O_{(S)} + 2Ur\phi_5 + V_2O_{5(V)} + 6H_2O_{(H)}$	80
	$Ni[(UO_2)_2(V_2O_8)](H_2O)_4$	$NiO_{(I)} + 2Ur\phi_5 + V_2O_{5(V)} + 4H_2O_{(H)}$	81
	$Cs_2[(UO_2)_2(V_2O_8)]$	$Cs_2O_{(I)} + 2Ur\phi_5 + V_2O_{5(V)}$	82
	$Cs_2[(UO_2)_2(Nb_2O_8)]$	$Cs_2O_{(I)} + 2Ur\phi_5 + Nb_2O_{5(V)}$	83
iriginite	$[(UO_2)(MoO_3OH)_2(H_2O)](H_2O)$	$2H_2O_{(S)} + Ur\phi_5 + 2MoO_{3(VI)} + H_2O_{(H)}$	84
	$[Ca(UO_2)Mo_4O_{14}]$	$CaO_{(VII)} + Ur\phi_5 + 4MoO_{3(VI)}$	85
umohoite	$[(UO_2)MoO_4)](H_2O)_4$	$Ur\phi_6 + MoO_{3(VIII)} + 4H_2O$	86
	α-$(UO_2)(MoO_4)(H_2O)_2$	$Ur\phi_5 + MoO_{3(IV)} + 2H_2O_{(H)}$	87
	$Sr(UO_2)_6(MoO_4)_7(H_2O)_{15}$	$SrO_{(VI)} + 6Ur\phi_5 + 7MoO_{3(IV)} + 15H_2O_{(H)}$	88
	$Ba(UO_2)_3(MoO_4)_4(H_2O)_4$	$BaO_{(VI)} + 3Ur\phi_5 + 4MoO_{3(IV)} + 4H_2O_{(H)}$	89
	$Mg(UO_2)_3(MoO_4)_4(H_2O)_8$	$MgO_{(VI)} + 3Ur\phi_5 + 4MoO_{3(IV)} + 8H_2O_{(H)}$	90

Notes: 1. Taylor 1971; 2. Taylor and Banister 1972; 3. Siegel et al. 1972; 4. Finch et al. 1996; 5. inferred from Finch et al. 1996; 6. Hoeckstra and Siegel 1973; 7. Gebert et al. 1978; 8. Reshetov and Kovba 1966; 9. Kovba 1971; 10. Wolf and Hoppe 1986; 11. Kovba et al. 1958; 12. Van Egmond and Cordfunke 1976; 13. Saine 1989; 14. Kovba 1972; 15. Van Egmond 1976; 16. assumed to be similar to that of K_2UO_4 and Ce_2UO_4; 17. Pagoaga et al. 1987; 18. Loopstra and Rietveld 1969; 19. Cordfuke et al. 1991; 20. Reis et al.1976; 21. Allpress 1965; 22. Zachariasen 1954; 23. Cremers et al. 1986; 24. Piret 1985; 25. Piret et al. 1983; 26. Taylor et al. 1981; 27. Ginderow 1988; 28. Burns 1998; 29. Rosenzweig and Ryan 1975; 30. Ryan and Rosenzweig 1977; 31. Rosenzweig and Ryan 1977; 32. Viswanathan and Harneit 1986; 33. Demartin et al. 1992; 34. Baturin and Sidorenko 1985; 35. Morosin 1978; 36. Demartin et al. 1991; 37. Fitch and Cole 1991; 38. Linde et al. 1978; 39. Linde et al. 1984; 40. Miller and Taylor 1986; 41. Makarov and Ivanov 1960; 42. Khosrawan-Sazedj 1982a; 43. Piret and Declercq 1983; 44. Khosrawan-Sazedj 1982b; 45. Linde et al. 1980; 46. Atencio et al. 1991; 47. Piret et al. 1979; 48. Piret and Deliens 1987; 49. Stergiou et al. 1993; 50. Hanic 1960; 51. Ross and Evans 1964; 52. Brandenburg and Loopstra 1973; 53. Van der Putten and Loopstra 1974; 54. Assumed to be similar to $UO_2SO_4{\cdot}2.5H_2O$ and $UO_2SO_4{\cdot}3.5H_2O$; 55. Brandenburg and Loopstra 1978; 56. Ross and Evans 1960; 57. Serezhkin et al. 1981; 58. Alcock et al. 1982; 59. Niinisto et al. 1979; 60. Vochten et al. 1995; 61. Christ et al. 1955; 62. Mereiter 1982; 63. Mayer and Mereiter 1986; 64. Mereiter 1986a; 65. Mereiter 1986b; 66. Mereiter 1988; 67. Mereiter 1986c; 68. Zalkin et al. 1989; 69. Taylor and Mueller 1965; 70. Dalley et al. 1971; 71. Perrin 1976; 72. Aberg 1978; 73. Gasperin 1988; 74. Gasperin 1990; 75. Gasperin 1987c; 76. Gasperin 1987b; 77. Mereiter 1986d; 78. Borene and Cesbron 1971; 79. Appleman and Evans 1965; 80. Piret et al. 1980; 81. Borene and Cesbron 1970; 82. Dickens et al. 1992; 83. Gasperin 1987a; 84. Serezhkin et al. 1973; 85. Lee and Jaulmes 1987; 86. Makarov and Anikna 1963; 87. Serezhkin et al 1980; 88. Tabachenko et al. 1984b; 89. Tabachenko et al. 1984a; 90. Tabachenko et al. 1983.

DATABASE

Grenthe et al. (1992) have completed a comprehensive review of the literature of thermodynamic data for uranium and have developed a database of uranium species, including some U^{6+} minerals, for use in safety assessments of radioactive waste repositories. This database has been widely adopted among chemists and geochemists, and, when available, the ΔG_f^0 and ΔH_f^0 data used in the regression analysis of the present study for deriving the contributions of fictive structural components have been adopted from Grenthe et al. (1992). We note that (1) the thermodynamic properties of fictive "cation oxides" in structures are quite different from those of pure oxides, as has been demonstrated for silicate minerals (Chermak and Rimstidt 1989); (2) α–UO_3 contains distorted polyhedra and studied samples may not have had the exact stoichiometry of $UO_{3.00}$ (Loopstra and Cordfunke 1966); and (3) β-UO_3 and γ-UO_3 do not contain the uranyl ion, with the U^{6+} cation being coordinated in some other way, and the polyhedra are highly irregular (Debets 1966; Loopstra et al. 1977). Thus the ΔG_f^0 and ΔH_f^0 of the simple oxides for U^{6+} were not included in the model data. Because the thermodynamic properties of a fictive component calculated in this way represent average contributions of

the component to the relevant properties of uranyl solid phases, thermodynamic data of phases with irregular structures (e.g., containing highly distorted polyhedra; involving U^{6+} cations not combined with oxygen anions to form uranyl cations) were not included in the model database. Only data for those phases for which the crystal structures are known were used in this study.

Data for uranyl silicates are notably absent from the limited amount of ΔG_f^0 and ΔH_f^0 data for U^{6+} compounds given by Grenthe et al. (1992). In recent years, new solubility data have been published for some uranyl phases (Nguyen et al. 1992; Moll et al. 1996; Casas et al. 1997b). Based on a review on these solubility data, we have calculated the $\Delta G^0_{f,298.15}$ values for soddyite, uranophane, Na-boltwoodite, and Na-weeksite to be -3653.0±2.8 kJ/mol, –6192.3 ± 3.4 kJ/mol, –2844.8 ± 3.9 kJ/mol, and –7993.9 ± 9.8 kJ/mol, respectively (Appendix 1).

Vochten and Van Haverbeke (1990) have performed solubility experiments on synthetic becquerelite and billietite. Assuming stoichiometric dissolution of the solid phases and based on the reaction: $M[(UO_2)_6O_4(OH)_6]\cdot 8H_2O + 14H^+ = M^{2+} + 6UO_2^{2+} + 18H_2O$ (M = Ba, Ca), our recalculation yielded log K_{SP} values of 40.11 and 36.07 for becquerelite and billietite, respectively, using Ca and Ba determinations in the fluid and the uranium database of Grenthe et al. (1992). The log K_{SP} value of 40.11 for becquerelite is in fair agreement with that reported by Sandino and Grambow (1994). However, Casas et al. (1997a) reported a log K_{SP} value of 29 ± 1 for becquerelite based on the solubility data for a natural becquerelite. Because this discrepancy is very large and no reasonable explanation is available, no thermodynamic datum for becquerelite was selected in the model database of this study.

The formula of billietite suggested by structural refinement (Pagoaga et al. 1987) is $Ba[(UO_2)_6O_4(OH)_6]\cdot 4H_2O$. A $\Delta G^0_{f,298}$ value of -9387.0 ± 17.1 kJ/mol for billietite was calculated based on this formula and the solubility data given by Vochten and Haverbeke (1990). This value is used in the present study.

Although each type of cation polyhedron is considered to possess a set of well-defined properties, the linkage topology of the polyhedra can also account for a few percent of the variation of thermodynamic properties for a particular type of cation polyhedron from structure to structure (Hazen 1985, 1988). Notably, the anion topology for the sheets of phases $M_XU_2O_7$ (M = K, Rb, Ca, and Sr; X = 1 or 2) contains only hexagons, and each hexagon is populated with a uranyl cation to form a hexa-bipyramid with each edge of the hexagon in the plane of the sheet being shared with neighboring polyhedra (Burns et al. 1996). The linkage between the cation polyhedra within sheets of this type of structure is much stronger than that found in other sheet structures of U^{6+} phases. In the course of the present analysis, we have found that the $\Delta G^0_{f,298}$ and $\Delta H^0_{f,298}$ values for phases with this structure type are always more negative than predicted. Because few phases possess this kind of structure, we suggest that thermodynamic properties of these phases be neither used in the reference database nor predicted using the present empirical method. Because the structures of most uranyl phases are based upon infinite sheets of polyhedra (Burns et al. 1996) and the prediction will be improved if the estimation is made within the phases that are structurally more analogous, uranyl phases containing isolated uranyl polyhedra were also not included in the model. Table 2 lists the thermodynamic data used to calculate g_i and h_i values in this study.

TABLE 2. Thermodynamic data used to calculate the g_i and h_i values listed in columns 1 and 3 of Table 3

Phases	$\Delta G^0_{f,298}$ (kJ/mol)	$\Delta H^0_{f,298}$ (kJ/mol)
$[(UO_2)_8O_2(OH)_{12}]\cdot 10H_2O$	–13092.0 ± 6.8	–14608.8 ± 13.6
β–$UO_2(OH)_2$	–1398.7 ± 1.8	–1533.8 ± 1.3
γ–$UO_2(OH)_2$		–1531.4 ± 1.3
$UO_3\cdot 0.9H_2O$	–1374.6 ± 2.5	–1506.3 ± 1.3
$Na_2U_2O_7$	–3011.5 ± 4.0	–3023.8 ± 1.8*
$Na_4UO_2(CO_3)_3$	–3737.8 ± 2.3	
UO_2CO_3	–1563.0 ± 1.8	–1689.65 ± 1.8*
$BaUO_4$	–1883.8 ± 3.4	–1993.8 ± 3.3
BaU_2O_7	–3052.1 ± 6.7	–3237.2 ± 5.0
$UO_2(NO_3)_2\cdot 6H_2O$	–2584.2 ± 1.6	–3167.5 ± 1.5
$UO_2(NO_3)_2\cdot 3H_2O$	–1864.7 ± 2.0	–2280.4 ± 1.7
$UO_2(NO_3)_2\cdot 2H_2O$	–1620.5 ± 2.0	–1978.7 ± 2.0
$UO_2SO_4\cdot 3.5H_2O$	–2535.6 ± 1.8	–2901.6 ± 0.8
$UO_2SO_4\cdot 3H_2O$	–2416.6 ± 1.8	–2751.5 ± 4.6
$UO_2SO_4\cdot 2.5H_2O$	–2298.5 ± 1.8	–2607.0 ± 0.9
$(UO_2)_2SiO_4\cdot 2H_2O$	–3655.7 ± 7.6†	
$Na(UO_2)(SiO_3OH)\cdot 1.5H_2O$	–2844.8 ± 3.9†	
$Na_2(UO_2)_2(Si_5O_{13})\cdot 3H_2O$	–7993.9 ± 9.6†	
$Ba(UO_2)_6O_4(OH)_6\cdot 4H_2O$	–9387.0 ± 17.1†	
Li_2UO_4	–1853.2 ± 2.2*	–1968.2 ± 1.3
$Li_2U_3O_{10}$		–4437.4 ± 4.1
$MgUO_4$	–1749.6 ± 1.5*	–1857.30 ± 1.5*
$Ca[(UO_2)(SiO_3OH)]_2\cdot 5H_2O$	–6192.3 ± 3.4*†	
$UO_2HPO_4\cdot 4H_2O$	–3064.75 ± 2.4*	–3469.97 ± 7.8*
K_2UO_4	–1798.50 ± 3.25*	–1920.70 ± 2.2*
Rb_2UO_4	–1800.14 ± 3.25*	–1922.70 ± 2.2*
Cs_2UO_4	–1805.37 ± 1.23*	–1928.00 ± 1.2*

*Not used in the regression analysis, instead, each value is used to calculate a g_i or h_i value for one component based on the regression results; the other data are used in the regression analysis to obtain the g_i and h_i values listed in columns 1 and 3 of Table 3, respectively.
†Calculated based on the solubility data reported by Vochten and Haverbeke (1990), Nguyen et al. (1992), Moll et al. (1996), and Casas et al. (1997b); others are from Grenthe et al. (1992)

CALCULATION METHODS AND LIMITATIONS OF DATABASE

The constituent structural components for 27 phases (listed in Table 2) for which the ΔG_f^0 and/or ΔH_f^0 values were used in the calculations are given in Table 1. Regression analysis was used to determine the molar contributions of structural components (g_i and h_i) to ΔG_f^0 and ΔH_f^0 of U^{6+} phases for the following models: $\Delta G_f^0 = S n_i g_i$ and $\Delta H_f^0 = S n_i h_i$, where n_i is the number of moles of component i. The g_i or h_i of the components that occur in at least two phases for which the relevant thermodynamic data (ΔG_f^0 or DH_f^0) and structural information are available were included in the predictor variables of the regression analysis. Thus, the $\Delta G_{f,298}^0$ values of 18 phases in Table 2 can be used in the simultaneous determination of the molar contribution (g_i) of $Ur\phi_4$, $Ur\phi_5$, $Ur\phi_6$, $Na_2O_{(I)}$, $BaO_{(I)}$, $CO_{2(III)}$, $N_2O_{5(III)}$, $SO_{3(IV)}$, $SiO_{2(IV)}$, $H_2O_{(S)}$, and $H_2O_{(H)}$ to ΔG_f^0 of U^{6+} phases, and the $\Delta H_{f,298}^0$ of 14 phases in Table 2 can be used to determine by regression the molar contribution (h_i) of $Ur\phi_4$, $Ur\phi_6$, $Li_2O_{(I)}$, $BaO_{(I)}$, $N_2O_{5(III)}$, $SO_{3(IV)}$, $H_2O_{(S)}$, $H_2O_{(H)}$ to the $\Delta H_{f,298}^0$ of U^{6+} phases. However, no significant differences exist among the calculated g_i or h_i values for different uranyl polyhedron types ($Ur\phi_4$, $Ur\phi_5$ and $Ur\phi_6$), and the result is rather sensitive to the change of the data used in the model. Because those phases that contain highly distorted or unusual polyhedra are excluded from the model, the number of the equatorial <U^{6+}-O> bonds and their bond-strengths generally depend on coordination number. Thus, differences are to be expected among the g_i or h_i values of different types of uranyl coordination polyhedron. We suspect significant differences will be demonstrated when the model database is enlarged. The sensitivity of the regression result to the variation of the data used in the model depends on the ratio of the number of data and predictive variables. Enlarging the database or reducing the number of variables will make the result less sensitive to the change of the data used in the regression, as is demonstrated by taking the three types of uranyl coordination polyhedra as a single component to reduce the number of predictive variables. Thus, when the database is small, this treatment makes the result more reliable. For the present calculations the different uranyl polyhedra are considered as a single component, as long as no significant differences occur among the calculated g_i and h_i values for the different uranyl polyhedron types. The different uranyl polyhedra can be considered separately as soon as additional data are available. To avoid under- or over-weighting of the contribution of a particular phase, the number of U^{6+} polyhedra (the sum of $Ur\phi_4$, $Ur\phi_5$, and $Ur\phi_6$) for an individual mineral in the regression model was normalized to 1.0.

Based on the regression results, the molar contribution of other selected structural components to $\Delta G_{f,298}^0$ or $\Delta H_{f,298}^0$ of uranyl phases was calculated for each mineral for each component, because each of these structural components were contained in only one phase for which the crystal structure and $\Delta G^0_{f,298}$ or $\Delta H^0_{f,298}$ have been determined experimentally. All the thermodynamic data used to calculate the g_i and h_i values in this way are also listed in Table 2. The g_i of $Li_2O_{(I)}$, $K_2O_{(I)}$, $Rb_2O_{(I)}$, $Cs_2O_{(I)}$, $CaO_{(I)}$, $MgO_{(I)}$, and $P_2O_{5(IV)}$ were calculated, respectively, using the $\Delta G^0_{f,298}$ of Li_2UO_4, K_2UO_4, Rb_2UO_4, Cs_2UO_4, $Ca[(UO_2)(SiO_3OH)]_2(H_2O)_5$ (uranophane), $MgUO_4$, and $(UO_2)HPO_4{\cdot}4H_2O$, whereas the h_i for $Na_2O_{(I)}$, $K_2O_{(I)}$, $Rb_2O_{(I)}$, $Cs_2O_{(I)}$, $MgO_{(I)}$, $CO_{2(III)}$, and $P_2O_{5(IV)}$ were obtained from the $\Delta H_{f,298}^0$ of $Na_2U_2O_7$, K_2UO_4, Rb_2UO_4, Cs_2UO_4, $MgUO_4$, UO_2CO_3, and $(UO_2)HPO_4{\cdot}4H_2O$, respectively. For example, the structural components of uranophane are $CaO_{(I)}$ + $2Ur\phi_5$ + $2SiO_{2(IV)}$ + $H_2O_{(S)}$ + $5H_2O_{(H)}$. Thus, the g_i value of $CaO_{(I)}$ can be calculated by: g_i [$CaO_{(I)}$] = ΔG_f^0 [uranophane] - {$2g_i$ [$Ur\phi_5$] + $2g_i$ [$SiO_{2(IV)}$] + g_i [$H_2O_{(S)}$] + $5g_i$ [$H_2O_{(H)}$]}. All the g_i values for the components on the left side are obtained by multiple regression analysis, but the errors in the ΔG_f^0 value of uranophane will propagate through the derived g_i of $CaO_{(I)}$. Because this kind of calculation includes error propagation and the phase used in the calculation may not be representative due to structural variations among the phases, the error in the prediction using the g_i or h_i values calculated in this way may be large.

RESULTS

The g_i and h_i values derived from the regression model are listed in Table 3. The data used to calculate the g_i and h_i values listed in columns 1 and 3 are listed in Table 2. The average differences between the predicted and the measured values for the phases used in the regression analysis are 0.095% for $\Delta G_{f,298}^0$ and 0.09% for $\Delta H_{f,298}^0$, and these differences are normally distributed when the number of uranyl cations in the formula is normalized to 1.0. The average reported associated errors (2σ) of experimentally determined data for silicate minerals are 0.16% for ΔG_f^0 and 0.13% for ΔH_f^0 (Chermak and Rimstidt 1989), and those for U^{6+} minerals are slightly higher. Thus, the associated errors for the predicted $\Delta G_{f,298}^0$ and $\Delta H_{f,298}^0$ values are generally below those of the experimentally determined values within the model database.

As a blind test, Table 4 lists the measured and predicted $\Delta G_{f,298}^0$ values for uranyl phases that were not used in the development of the database for the model. The measured $\Delta G_{f,298}^0$ values for the uranyl phosphates were selected by Grenthe et al. (1992) in the uranium thermodynamic database, but their crystal structures remain unknown. The difference between the measured and predicted values for anhydrous uranyl phosphate, $(UO_2)_3(PO_4)_2$, is 0.32% and may result mainly from the uncertainty of g_i for $PO_{4(IV)}$, which was calculated using the $\Delta G_{f,298}^0$ value of $UO_2HPO_4{\cdot}4H_2O$ by the error propagation method. From the difference between the measured $\Delta G_{f,298}^0$ values of $(UO_2)_3(PO_4)_2{\cdot}6H_2O$ and $(UO_2)_3(PO_4)_2{\cdot}4H_2O$, we obtain the molar contribution of molecular water ($H_2O_{(H)}$) to the $\Delta G_{f,298}^0$ of uranyl phosphates as -239.5 KJ/mol, which agrees with that obtained by the multi-regression analysis (listed in Table 3). However, the difference between the measured $\Delta G_{f,298}^0$ values of $(UO_2)_3(PO_4)_2{\cdot}4H_2O$ and $(UO_2)_3(PO_4)_2$ is –1023 kJ/mol, indicating that the molar contribution of molecular water to the $\Delta G_{f,298}^0$ of uranyl phosphates is –255.75 kJ/mol. This discrepancy accounts for the large residual of the predicted $\Delta G_{f,298}^0$ values for $(UO_2)_3(PO_4)_2{\cdot}4H_2O$ and $(UO_2)_3(PO_4)_2{\cdot}6H_2O$, and experimental studies are needed to explain this discrepancy. Probable sources of this discrepancy include (1) the structure of $(UO_2)_3(PO_4)_2{\cdot}4H_2O$ and $(UO_2)_3(PO_4)_2{\cdot}6H_2O$ are similar to each other but quite different from that of $(UO_2)_3(PO_4)_2$; (2) the number of water molecules in the samples may not be equal to their nominal stoichiometries; (3) the $\Delta G_{f,298}^0$ value of $(UO_2)_3(PO_4)_2{\cdot}4H_2O$ is in error

TABLE 3. The molar contribution (g_i and h_i) of structural components to $\Delta G^0_{f,298}$ and $\Delta H^0_{f,298}$ of U^{6+} phases

	g_i (kJ/mol)		h_i (kJ/mol)	
Component	1	2	3	4
UO_3	–1162.18	–1161.05	–1237.73	–1233.75
$Na_2O_{(I)}$	–688.59	–686.54	–728.34*	–736.30*
$MgO_{(I)}$	–587.42*	–589.17	–619.57*	–623.38
$CaO_{(I)}$	–722.72*	–715.77		–726.57
$BaO_{(I)}$	–724.46	–725.91	–757.21	–761.98
$SiO_{2(IV)}$	–853.32	–853.96		
$SO_{3(IV)}$	–540.27	–538.87	–629.30	–624.17
$CO_{2(III)}$	–400.15	–400.61	–451.87*	–455.59
$N_2O_{5(III)}$	20.16	21.95	–75.71	–78.99
$P_2O_{5(IV)}$	–1645.66*	–1638.25	–1799.14*	–1802.37
$H_2O_{(S)}$	–237.08	–237.94	–295.02	–299.93
$H_2O_{(H)}$	–240.30	–241.10	–296.29	–295.58
$Li_2O_{(I)}$	–691.01*	–692.14*	–729.22	–737.75
$K_2O_{(I)}$	–636.32*	–637.45*	–682.97*	–686.95*
$Rb_2O_{(I)}$	–637.92*	–639.05*	–684.97*	–688.95*
$Cs_2O_{(I)}$	–643.22*	–644.35*	–690.27*	–694.25*

*Calculated for a single phase for one component using the corresponding datum of the specific phase (see description in the text). Other values are obtained by multiple linear regression analysis. The thermodynamic data used to calculate the g_i and h_i values listed in columns 1 and 3, respectively, are listed in Table 2; and the model data listed in Tables 6 and 8 were used, respectively, in the regression analysis to obtain the relevant g_i and h_i values listed in columns 2 and 4. Columns 2 and 4 are revised g_i and h_i values, respectively, obtained by adding data into the model data base (see discussions in text).

(the "measured" $\Delta G^0_{f,298}$ value of $(UO_2)_3(PO_4)_2{\cdot}6H_2O$ was estimated based on that of $(UO_2)_3(PO_4)_2{\cdot}4H_2O$.

The structural components for liebigite $[Ca_2(UO_2)(CO_3)_3{\cdot}11H_2O]$, swartzite $[CaMg(UO_2)(CO_3)_3{\cdot}12H_2O]$, bayleyite $[Mg_2(UO_2)(CO_3)_3{\cdot}18H_2O]$, and andersonite $[Na_2Ca(UO_2)(CO_3)_3{\cdot}6H_2O]$ have been given in Table 1, and their Gibbs free energies of formation were reported by Alwan and Williams (1980) based on solubility determinations at five different temperatures in the range of 0 to 21 °C. Because no detailed solubility data were given and there were serious calculation errors in the original paper, Grenthe et al. (1992) considered the thermodynamic data reported by Alwan and Williams (1980) for these liebigite group minerals unreliable. Using the solubility products reported by Alwan and Williams (1980) and the auxiliary data of Grenthe et al. (1992) for the ions involved, we recalculated the ΔG^0_f of these uranyl carbonates with the same uncertainties as reported in the original paper. Despite the fact that the g_i values of $CaO_{(I)}$ and $MgO_{(I)}$ were obtained for one mineral for one component using error propagationmethod , the predicted $\Delta G^0_{f,298}$ values are in fair agreement with the measured values (Table 4). We suspect that the larger residual of the predicted $\Delta G^0_{f,298}$ value for liebigite results mainly from the uncertainty in the g_i value of $CaO_{(I)}$ and the errors in the experiment. Adding the $\Delta G^0_{f,298}$ values of swartzite, bayleyite, andersonite, uranophane, $(UO_2)HPO_4{\cdot}4H_2O$, and $(UO_2)_3(PO_4)_2$ into the model database, the regression analysis resulted in an average residual of 0.08% (Table 5) and a set of improved g_i values for the structural components (Table 3, column 2). This result suggests that the $\Delta G^0_{f,298}$ values for swartzite, bayleyite, and andersonite recalculated in the present study based on the solubility data reported by Alwan and Williams (1980) might be good approximations of their ΔG^0_f, and the solubility product of liebigite may be erroneous.

Table 6 lists the measured and predicted $\Delta H^0_{f,298}$ values for selected uranyl phases that were not used in the development of the database for the model. Similar to the case for $\Delta G^0_{f,298}$, the predicted $\Delta H^0_{f,298}$ value of $(UO_2)HPO_4{\cdot}4H_2O$ is also much more positive than that measured, and similar explanations are applicable. The $\Delta H^0_{f,298}$ values for the four liebigite-group minerals were also recalculated using the respective dissolution enthalpies of these minerals reported by Alwan and Williams (1980) and using the $\Delta H^0_{f,298}$ values for the relevant aqueous species provided by Grenthe et al. (1992). There are two Ca-bearing phases ($CaUO_4$ and Ca_3UO_6) for which the measured $\Delta H^0_{f,298}$ values were available. As indicated previously, the linkage between the cation polyhedra within the sheets in the structure of $CaUO_4$ is much stronger than that in the structures of the uranyl phases used in the model. Thus, the $\Delta G^0_{f,298}$ and $\Delta H^0_{f,298}$ values for $CaUO_4$ are more negative than those predicted (Table 7). However, Ca_3UO_6 is based on a structure containing isolated $U\phi_4$ polyhedra and the linkage between the cation polyhedra is much weaker than that in the phases based on sheet structures. Thus, the $\Delta G^0_{f,298}$ and $\Delta H^0_{f,298}$ values for Ca_3UO_6 should be more positive than those predicted. The h_i values of $CaO_{(I)}$ calculated based on the $\Delta H^0_{f,298}$ values of $CaUO_4$ and Ca_3UO_6 are –764.6 kJ/mol and –689.2 kJ/mol, respectively. Therefore, these two values were averaged to obtain a rough estimation of the h_i of $CaO_{(I)}$ (–726.9 kJ/mol), which was used to calculate the pre-

TABLE 4. Measured and predicted $\Delta G^0_{f,298}$ values for the uranyl phases not used in the model and the related residuals

Phases	Measured (kJ/mol)	Predicted (kJ/mol)	Residuals (kJ/mol)	Percent residuals
$(UO_2)_3(PO_4)_2$	–5116.0 ± 5.5	–5132.2	16.2	0.32
$(UO_2)_3(PO_4)_2{\cdot}4H_2O$	–6139.0 ± 6.4	–6093.4	–45.6	0.74
$(UO_2)_3(PO_4)_2{\cdot}6H_2O$	–6618.0 ± 7.0	–6574.0	–44	0.66
$Ca_2(UO_2)(CO_3)_3{\cdot}11H_2O$	–6418.8 ± 12	–6452.2	33.4	0.52
$CaMg(UO_2)(CO_3)_3{\cdot}12H_2O$	–6561.4 ± 8	–6556.4	–5.0	0.07
$Mg_2(UO_2)(CO_3)_3{\cdot}18H_2O$	–7881.1 ± 8	–7862.9	–18.2	0.23
$Na_2Ca(UO_2)(CO_3)_3{\cdot}6H_2O$	–5207.1 ± 24	–5215.7	8.64	0.17

Note: The measured values for the uranyl phosphates are from Grenthe et al. (1992); and the measured values for the liebigite group minerals were calculated based on the solubility data reported by Alwan and Williams (1980).

TABLE 5. Measured and predicted $\Delta G^0_{f,298}$ values for the uranyl phases after adding data to the model and the related residuals

Phases	Measured (kJ/mol)	Predicted (kJ/mol)	Residuals (kJ/mol)	Percent residuals
$[(UO_2)_8O_2(OH)_{12}]\cdot 10H_2O$	–13092.0 ± 6.8	–13127.1	35.1	0.27
β-$UO_2(OH)_2$	–1398.7 ± 1.8	–1399.0	0.3	0.02
$UO_3\cdot 0.9H_2O$	–1374.6 ± 2.5	–1375.2	0.6	0.04
$Na_2U_2O_7$	–3011.5 ± 4.0	–3008.6	–2.9	0.09
$Na_4UO_2(CO_3)_3$	–3737.8 ± 2.3	–3735.9	–1.86	0.05
UO_2CO_3	–1563.0 ± 1.8	–1561.7	–1.3	0.09
$BaUO_4$	–1883.8 ± 3.4	–1887.0	3.2	0.17
BaU_2O_7	–3052.1 ± 6.7	–3048.0	–4.1	0.13
$MgUO_4$	–1749.6 ± 1.5	–1750.2	0.6	0.04
$UO_2(NO_3)_2\cdot 6H_2O$	–2584.2 ± 1.6	–2585.7	1.5	0.06
$UO_2(NO_3)_2\cdot 3H_2O$	–1864.7 ± 2.0	–1862.4	–2.3	0.12
$UO_2(NO_3)_2\cdot 2H_2O$	–1620.5 ± 2.0	–1621.3	0.8	0.05
$UO_2SO_4\cdot 3.5H_2O$	–2535.6 ± 1.8	–2537.5	1.9	0.07
$UO_2SO_4\cdot 3H_2O$	–2416.6 ± 1.8	–2416.9	0.3	0.01
$UO_2SO_4\cdot 2.5H_2O$	–2298.5 ± 1.8	–2296.4	–2.2	0.09
$(UO_2)_2SiO_4\cdot 2H_2O$	–3652.8 ± 2.8	–3652.0	–0.8	0.02
$Na(UO_2)(SiO_3OH)\cdot 1.5H_2O$	–2844.8 ± 3.9	–2838.9	–5.9	0.21
$Na_2(UO_2)_2(Si_5O_{13})\cdot 3H_2O$	–7993.9 ± 9.6	–8001.8	7.9	0.10
$Ba(UO_2)_6O_4(OH)_6\cdot 4H_2O$	–9387.0 ± 17.1	–9370.4	–16.6	0.18
$Ca[(UO_2)(SiO_3OH)]_2\cdot 5H_2O$	–6192.3 ± 3.4	–6189.2	–3.1	0.05
$(UO_2)_2HPO_4\cdot 4H_2O$	–3064.7 ± 2.4	–3063.5	–1.2	0.04
$(UO_2)_3(PO_4)_2$	–5116.0 ± 5.5	–5121.4	5.3	0.11
$CaMg(UO_2)(CO_3)_3\cdot 12H_2O$	–6561.4 ± 8	–6561.0	–0.4	0.01
$Mg_2(UO_2)(CO_3)_3\cdot 18H_2O$	–7881.1 ± 8	–7881.0	0.1	0.00
$Na_2Ca(UO_2)(CO_3)_3\cdot 6H_2O$	–5207.1 ± 24	–5211.8	–4.7	0.09
Average				0.08

Note: See Tables 2 and 4 for the sources of the measured $\Delta G^0_{f,298}$ values.

TABLE 6. Measured and predicted $\Delta H^0_{f,298}$ values for uranyl phases not used in the model and the associated residuals

Phases	Measured (kJ/mol)	Predicted (kJ/mol)	Residuals (kJ/mol)	Percent residuals
$(UO_2)_3(PO_4)_2$	–5491.3 ± 3.5*	–5512.3	21.0	0.38
$(UO_2)_3(PO_4)_2\cdot 4H_2O$	–6739.1 ± 9.1*	–6690.9	–48.2	0.72
$Ca_2(UO_2)(CO_3)_3\cdot 11H_2O$	–7301.6 ± 24	–7306.3	4.7	0.06
$CaMg(UO_2)(CO_3)_3\cdot 12H_2O$	–7504.4 ± 20	–7495.3	–9.1	0.12
$Mg_2(UO_2)(CO_3)_3\cdot 18H_2O$	–9164.2 ± 20	–9165.7	1.5	0.02
$Na_2Ca(UO_2)(CO_3)_3\cdot 6H_2O$	–5893.0 ± 36	–5826.3	–53.1	1.13
$Li_2U_2O_7$	–3213.6 ± 5.3*	–3024.7	–8.9	0.28

* From Grenthe et al. (1992); the measured $\Delta H^0_{f,298}$ data for the liebigite group uranyl carbonates were calculated based on the dissolution enthalpy data reported by Alwan and Williams (1980).

dicted $\Delta H^0_{f,298}$ values of the liebigite group minerals listed in Table 6. For liebigite, swartzite, and bayleyite, the predicted $\Delta H^0_{f,298}$ values are in good agreement with those measured. Structural information and the calculations made in this study indicate that the prediction of the $\Delta G^0_{f,298}$ and $\Delta H^0_{f,298}$ for liegibite group minerals is rather reliable. Thus, the large difference between the predicted and measured $\Delta H^0_{f,298}$ values of andersonite suggests that the measured value may be in error, which is also indicated by the very large uncertainty of the measured value. The structure of $Li_2U_2O_7$ remains unknown, but the predicted $\Delta H^0_{f,298}$ value is in fair agreement with the measured value. Adding liebigite, swartzite, bayleyite, UO_2CO_3, $MgUO_4$, $UO_2HPO_4\cdot H_2O$, $(UO_2)_3(PO_4)_2$, and $Li_2U_2O_7$ to the model, the regression analysis of the $\Delta H^0_{f,298}$ values resulted in an average residual of 0.10% (Table 8) and a set of revised h_i values (Table 3, column 4).

The analysis described above demonstrates that this technique gives reliable predictions of the $\Delta G^0_{f,298}$ and $\Delta H^0_{f,298}$ for most uranyl phases, and the prediction can be improved immediately as accurately determined new data become available.

Finally, we have identified some phases for which the $\Delta G^0_{f,298}$ and $\Delta H^0_{f,298}$ could not be predicted reliably using the model presented here, but the deviation can be explained based on structural information (available examples are listed in Table 7). These phases fall into three structure types according to the structural classification of uranyl phases by Burns et al. (1996). The first type is based on a sheet structure and includes the phases $M_xU_2O_7$ (M = K, Rb, Ca, Sr; x = 1 or 2). The anion topology of the sheets contains only hexagons, and each hexagon is populated with a uranyl cation to form a hexa-bipyramid with all the edges of the hexagon in the plane of the sheet being shared with neighboring hexagons. The strong linkage between the cation polyhedra within the sheets makes the measured $\Delta G^0_{f,298}$ and $\Delta H^0_{f,298}$ values for the phases of this class more negative than those predicted (Table 8). The second type is based on a chain structure in which the chains contain only uranyl polyhedra and are formed by sharing single corners between $Ur\phi_4$ polyhedra. The linkage between the cation polyhedra in this type of structure is generally much weaker than that in most uranyl phases. Phases belonging to this class are Na_4UO_5, Li_4UO_5, Ca_2UO_5, and Sr_2UO_5. The third class includes those phases consisting of isolated cation polyhedra (e.g., Sr_3UO_6

TABLE 7. Phases for which the model predictions were not reliable based on their structural description

Phases	$\Delta G^0_{f,298}$ (kJ·mol^{-1})		$\Delta H^0_{f,298}$ (kJ·mol^{-1})	
	Measured	Predicted	Measured	Predicted
$CaUO_4$	–1888.7	–1876.8	–2002.3	–1960.3
$K_2U_2O_7$			–3250.5	–3154.5
$Rb_2U_2O_7$			–3232.0	–3156.5
Li_4UO_5			–2639.4	–2709.3
Na_4UO_5			–2456.6	–2706.4
Ca_3UO_6			–3305.4	–3413.5

Note: The measured values are from Grenthe et al. (1992).

TABLE 8. Measured and predicted $\Delta H^0_{f,298}$ values for uranyl phases after adding data to the model and the related residuals

Uranyl phases (kJ/mol)	Measured (kJ/mol)	Predicted (kJ/mol)	Residuals residuals	Percent
$[(UO_2)_8O_2(OH)_{12}]\cdot 10H_2O$	–14608.8 ± 13.6	–14625.4	16.6	0.11
β-$UO_2(OH)_2$	–1533.8 ± 1.3	–1533.7	–0.1	0.01
γ-$UO_2(OH)_2$	–1531.4 ± 1.3	–1533.7	2.3	0.15
$UO_3\cdot 0.9H_2O$	–1506.3 ± 1.3	–1503.7	–2.6	0.17
Li_2UO_4	–1968.2 ± 1.3	–1971.5	3.3	0.17
$Li_2U_2O_7$	–3213.6 ± 5.3	–3205.3	–8.3	0.26
$Li_2U_3O_{10}$	–4437.4 ± 4.1	–4439.0	1.6	0.04
$BaUO_4$	–1993.8 ± 3.3	–1995.7	1.9	0.10
BaU_2O_7	–3237.2 ± 5.0	–3229.5	–7.7	0.24
$UO_2(NO_3)_2\cdot 6H_2O$	–3167.5 ± 1.5	–3165.2	–2.3	0.07
$UO_2(NO_3)_2\cdot 3H_2O$	–2280.4 ± 1.7	–2278.5	–1.9	0.08
$UO_2(NO_3)_2\cdot 2H_2O$	–1978.7 ± 2.0	–1982.9	4.2	0.21
$UO_2SO_4\cdot 3.5H_2O$	–2901.6 ± 0.8	–2901.2	–0.4	0.02
$UO_2SO_4\cdot 3H_2O$	–2751.5 ± 4.6	–2753.4	1.9	0.07
$UO_2SO_4\cdot 2.5H_2O$	–2607.0 ± 0.9	–2605.6	–1.4	0.05
$UO_2HPO_4\cdot 4H_2O$	–3470.0 ± 7.8	–3467.2	–2.8	0.08
$(UO_2)_3(PO_4)_2$	–5491.3 ± 3.5	–5503.6	12.3	0.22
$MgUO_4$	–1857.3 ± 1.5	–1857.1	–0.2	0.01
$Ca_2(UO_2)(CO_3)_3\cdot 11H_2O$	–7301.6 ± 24	–7305.1	3.5	0.05
$MgCa(UO_2)(CO_3)_3\cdot 12H_2O$	–7504.4 ± 20	–7497.5	–6.9	0.09
$Mg_2(UO_2)(CO_3)_3\cdot 18H_2O$	–9164.2 ± 20	–9167.8	3.6	0.04
UO_2CO_3	–1689.6 ± 1.8	–1689.3	–0.3	0.02
Average				0.10

Note: See Tables 2 and 6 for the sources of the measured $\Delta H^0_{f,298}$ values.

and Ca_3UO_6). The weak connection between cation polyhedra in the second and third structure types makes the measured $\Delta G^0_{f,298}$ and $\Delta H^0_{f,298}$ values for these phases more positive than those predicted. The $\Delta H^0_{f,298}$ values for α-$SrUO_4$, β-$SrUO_4$, Sr_2UO_5, and Sr_3UO_6 are –1989.6 kJ/mol, –1990.8 kJ/mol, –2635.6 kJ/mol, and –3263.4 kJ/mol, respectively (Grenthe et al. 1992). The h_i values for $SrO_{(I)}$ calculated using these $\Delta H^0_{f,298}$ values are –755.85 kJ/mol, –757.05 kJ/mol, –700.93 kJ/mol, and –676.55 kJ/mol, respectively. These results agree with the structural interpretation that the connection between the cation polyhedra in α-$SrUO_4$ and β-$SrUO_4$ is much stronger than that in Sr_2UO_5 and Sr_3UO_6, as described above. Therefore, the h_i value for $SrO_{(I)}$ should be in the range of –700.93 kJ/mol to –755.85 kJ/mol.

To analyze further the reasonableness of the estimated $\Delta G^0_{f,298}$ values for U^{6+} phases, activity-activity diagrams for the CO_2-CaO-UO_3-H_2O, and SiO_2-CaO-UO_3-H_2O systems were constructed using the estimated $\Delta G^0_{f,298}$ values of this study. Representative groundwater compositions are plotted on the diagrams. The f_{CO_2} in the groundwater system represent the equilibrium fugacity of CO_2 calculated using the concentration of total carbonate in groundwater. The ΔG^0_f for the minerals used to construct the diagrams are listed in Table 9. Other thermodynamic data necessary to construct the activity-activity diagrams were taken from Grenthe et al. (1992). Although this method has several advantages over previous efforts, it is inadvisable to replace accurate experimental studies with empirical predictions (Tardy and Garrels 1974; Chermak and Rimstidt 1989). Therefore, in constructing the activity-activity diagrams, the predicted $\Delta G^0_{f,298}$ values were not used in cases for which reliable measured values are available.

In addition to thermodynamic stabilities, precipitation kinetics and crystal size and habit of solid phases can significantly affect their observed relations in nature. If the precipitation of a phase is unfavorable kinetically, a much higher degree of oversaturation is needed to overcome the nucleation barrier to precipitation; fine-grained crystals will contribute to the surface free energy and effectively increase the solubility of the solid phase. Distortion of the polyhedra or of the whole structure will create strain within the lattice, leading to a significant increase of the solubility of relevant phases; thus, the estimated Gibbs free energies for phases with an irregular structure may not be reliable.

TABLE 9. $\Delta G^0_{f,298}$ values for the U^{6+} minerals used in the construction of Figures 1 and 2 (kJ/mol)

Uranyl phases	Formula	This study	Finch (1997)	M/C*
metaschoepite	$[(UO_2)_8O_2(OH)_{12}]\cdot(H_2O)_{10}$	–13092.0	–13092.0	M
becquerelite	$Ca[(UO_2)_6O_4(OH)_6](H_2O)_8$	–10324.7	–10305.8	C
rutherfordine	UO_2CO_3	–1563.0	–1563.0	M
urancalcarite	$Ca_2[(UO_2)_3(CO_3)(OH)_6](H_2O)_3$	–6036.7	–6037.0	C
sharpite	$Ca[(UO_2)_6(CO_3)_5(OH)_4](H_2O)_6$	–11607.6	–11601.1	C
fontanite	$Ca[(UO_2)_3(CO_3)_4](H_2O)_3$	–6524.7	–6523.1	C
liebigite	$Ca_2[(UO_2)(CO_3)_3](H_2O)_{11}$	–6446.4	–6468.6	C
haiweeite	$Ca[(UO_2)_2(Si_2O_5)_3](H_2O)_5$	–9367.2	–9431.4	C
ursilite	$Ca_4[(UO_2)_4(Si_2O_5)_5(OH)_6](H_2O)_{15}$	–20377.4	–20504.6	C
soddyite	$[(UO_2)_2SiO_4](H_2O)_2$	–3653.0	–3658.0	M
uranophane	$Ca[(UO_2)(SiO_3OH)]_2(H_2O)_5$	–6192.3	–6210.6	M

*M/C indicates measured or calculated values. See Table 5 for the measured values used in the present study.

CO_2-CaO-UO_3-H_2O system

Among the uranyl phases found in the CO_2-CaO-UO_3-H_2O system, liebigite commonly occurs as extremely fined-grained efflorescences on mine walls, surface outcrops, and elsewhere where evaporation is high (Finch 1997); zellerite also forms fine-grained crystals in nature with an unknown structure. Thus, liebigite and zellerite are more soluble and less commonly found in nature than predicted using the empirical method. The strain in the structure of calciouranoite caused by structural limitations on the ability of the uranyl oxide hydrate sheets to accommodate a large amount of interlayer Ca makes it less stable (Finch 1994), and a similar argument may account for the absence of "Ca-protasite" as a naturally occurring phase. The estimated ΔG_f^0 for calciouranoite and "Ca-protasite" are, thus, not considered reliable. Therefore, liebigite, zellerite, calciouranoite, and "Ca-protasite" are excluded from the activity-activity diagram for the CO_2-CaO-UO_3-H_2O system (Fig. 1).

Becquerelite has a large stability field as shown in Figure 1, and most of the groundwater compositions plot within this field. Considering that groundwaters from both crystalline and carbonate terrains are usually not oversaturated with respect to calcite (Fig. 2), rutherfordine should be the most common uranyl carbonate, which is in agreement with the field observations (Frondel 1958). Because the f_{CO_2} necessary for the precipitation of rutherfordine, sharpite, and fontanite is high, it is almost impossible to achieve the required concentrations of carbonate species in groundwater systems. These minerals may form in half-closed systems where hydrostatic pressure and gas fugacity may be higher due to the weak hydraulic connection with the bulk groundwater system. Precipitation of urancalcarite is predicted to occur where the aqueous solution is oversaturated with respect to calcite, which is in agreement with its rare occurrence in deposits where the predominant carbonate minerals in the host rocks are magnesian calcite or dolomite (Deliens et al. 1981).

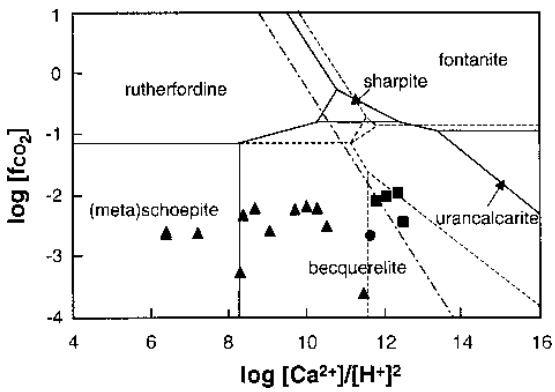

FIGURE 1. Activity-activity diagram for the system CO_2-CaO-UO_3-H_2O excluding liebigite, zellerite, calciouranoite, and "Ca-protacite," with the compositional plots for typical groundwaters (Freeze and Cherry 1979) from carbonate terrains (squares) and crystalline rocks (triangles) and for Yucca Mountain J-13 groundwater (circle; Bruton and Shaw 1988). Diagonal dot-dashed line represents calcite saturation. The mineral stability fields defined by the light dashed lines are based on the Gibbs free energies for the minerals given by Finch (1997) and listed in Table 9.

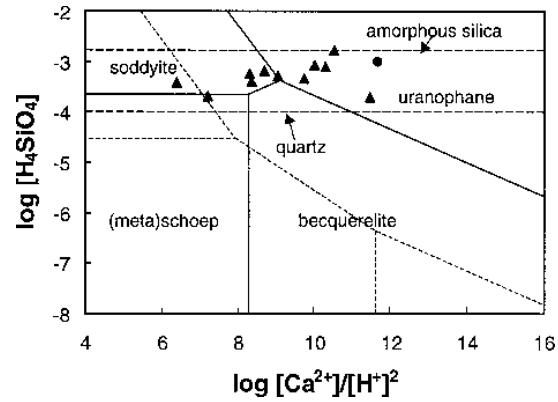

FIGURE 2. Activity-activity diagram for the system SiO_2-CaO-UO_3-H_2O constructed based on the $\Delta G_{f,298}^0$ values in Table 9 (excluding swanboite, uranosilite, haiweeite, and ursilite), with the compositional plots for typical groundwaters from crystalline rocks (triangle; Freeze and Cherry 1979) and for Yucca Mountain J-13 groundwater (circle; Bruton and Shaw 1988). Horizontal dashed lines represent quartz and amorphous silica equlibria. The mineral stability fields defined by the light dashed lines are based on the Gibbs free energies for the minerals given by Finch (1997) and listed in Table 9.

SiO_2-CaO-UO_3-H_2O system

From the unusual formula of swamboite, $U[(UO_2)(SiO_3OH)]_6(H_2O)_{30}$, one seventh of U^{6+} cations in the structure may be located in interlayer positions, not in structural units, and may not combine with O to form uranyl cations, but no analogous structure has been found in uranyl phases. In addition, there appears to be too many hydration water molecules relative to the number of cations in the formula. Thus, both the crystal structure and formula of swamboite are highly questionable. Because uranosilite has a molar ratio of UO_3/SiO_2 = 1:7, it is most probably based on a Si^{4+} tetrahedron-dominated structure, and the molar contributions of cation polyhedra to the $\Delta G_{f,298}^0$ and $\Delta H_{f,298}^0$ of uranosilite would be similar to those of silicate minerals. Therefore, the estimated $\Delta G_{f,298}^0$ of swamboite and uranosilite are considered unreliable and were not used in the construction of the activity-activity diagram.

Uranophane and soddyite are the most common minerals in oxidized uranium deposits where neither lead-bearing uranyl phases, nor uranyl phosphates are significant (Frondel 1958; Smith 1984; Pearcy et al. 1994). However, if haiweeite and ursilite are included in the log $[Ca^{2+}]/[H^+]^2$ vs. log$[H_4SiO_4]$ diagram for the SiO_2-CaO-UO_3-H_2O system (Fig. 2), the predicted stability fields for these phases replace most of the field for uranophane, with compositions of most groundwaters from crystalline rocks plotting in the field for haiweeite. Haiweeite and ursilite always form as fine-grained masses, and surface free energy must contribute to increasing the solubilities of these minerals. Thus, soddyite and uranophane may, in practice, be more stable than haiweeite and ursilite under most geochemical environments. Therefore, it is more informative to examine the stability relations among phases frequently found in nature, as illustrated in Figure 2. The chemical compositions of groundwaters from crystalline rocks plot in the stability field of soddyite and uranophane (Fig. 2).

The mineral stability relations predicted in this study and illustrated in Figures 1 and 2 suggest that (1) (meta)schoepite is unstable in groundwater systems and should mostly be replaced by soddyite and uranophane (Fig. 2), and may be replaced by becquerelite in a low silica system (Fig. 1); (2) soddyite and uranophane are more stable relative to other minerals included in Figure 2 in groundwaters from crystalline rocks; and (3) becquerelite may also precipitate from the groundwaters in crystalline rocks and be associated with soddyite and uranophane, although this may be a relatively rare occurrence. These conclusions are in agreement with the following field observations. (1) Although schoepite is common and may be kinetically favored early during the corrosion of uraninite, it is not usually abundant in most oxidized uranium deposits and is not a long-term solubility-limiting phase for UO_2^{2+} in natural groundwaters (Frondel 1958; Finch and Ewing 1992). (2) Soddyite and uranophane are among the most common U^{6+} minerals in oxidized uranium deposits (Frondel 1958; Smith 1984). And (3) becquerelite is the most common uranyl oxide hydrate mineral in nature (Frondel 1958) and is often found in association with soddyite and uranophane (Weeks and Thompson 1954; Frondel 1958; Pearcy et al. 1994).

In the activity-activity diagrams constructed using the $\Delta G^0_{f,298}$ values provided by Finch (1997) and listed in Table 9, the predicted stability field for liebigite is larger than that predicted in this study in the log $[Ca^{2+}]/[H^+]^2$ vs. log f_{CO_2} diagram; if ursilite and haiweeite were included in the diagram, they would have covered most of the entire field presented in Figure 2, with soddyite and uranophane being metastable phases. From similar activity-activity diagrams constructed by Finch (1997), which exclude the stability fields for liebigite, zellerite, haiweeite, uranosilite, and ursilite, it can be seen that: (1) most of the chemical compositions of groundwaters from crystalline rocks plot in the (meta)schoepite stability field instead of becquerelite stability field in Figure 1; (2) only for the cases in which the silica concentration in groundwater is lower than $10^{-6.35}$ mol will it be possible for becquerelite to precipitate; such a low silica concentration is not expected in the groundwaters from most rocks; and (3) it is highly unlikely that becquerelite will be found in association with rutherfordine and soddyite. However, becquerelite often occurs as an alteration mineral in uranium deposits located in sandstones, pyroclastic rocks, and intrusive igneous rocks (Frondel 1958; Weeks and Thompson 1954; Shoemaker 1956; Pearcy et al. 1994). Rutherfordine, and especially soddyite are among those phases typically associated with becquerelite. Thus, our predicted stability fields are in better agreement with described natural occurrences than that of Finch (1997).

APPLICATION TO SPENT NUCLEAR FUEL CORROSION

Uranyl phases are the solubility-limiting phases of uranium during the oxidative corrosion of spent nuclear fuel. Both the solution concentration of uranium and the secondary phase immobilization of actinides and fission products depend largely on the structure and stabilities of the secondary phases formed. Thus, a defensible predictive model for assessing the corrosion of spent fuel must be based on a critical examination of the phases that will be important during the process. Natural analogue studies suggest that the long-term paragenesis during the oxidative corrosion of UO_2 fuel can be summarized as (Frondel 1958; Finch and Ewing 1992): an initial decomposition of UO_2 to uranyl oxide hydrates followed by the formation of more stable uranyl silicates or, in phosphorous-rich groundwaters, the formation of uranyl phosphates. Because phosphorus is not expected to be present in significant amounts in spent nuclear fuel or in the groundwater of the proposed high-level waste repository at Yucca Mountain, uranyl silicates will most probably be the solubility-limiting phases for uranium. Among the uranyl silicates in the UO_3-CaO-SiO_2-H_2O system, haiweeite was suggested to be important during the oxidative corrosion of spent fuel by chemical simulation (Bruton and Shaw 1988) and experimental studies (Wilson 1988). Our prediction also indicates that haiweeite would be more stable in groundwaters from crystalline rocks. However, field observations indicate that uranophane is the most common uranyl silicate, and haiweeite is rare in nature. Because both the detailed structural information and thermodynamic data for haiweeite are not available, relevant experimental studies are highly recommended, and experiments combined with studies of natural occurrences are necessary to provide an explanation for this discrepancy and to determine whether the precipitation of haiweeite should be suppressed in geochemical models of the oxidative alteration of spent fuel. Becquerelite is potentially an important secondary mineral during the corrosion of spent fuel in repositories, but significant discrepancies exist in the solubility experiments and no calorimetric thermodynamic datum is available for becquerelite. Uranyl phosphates are among the most numerous and most commonly found uranyl phases in nature (Frondel 1958; Cejka and Urbanec 1990; Finch and Ewing 1992), but no thermodynamic data is available for the most abundant and structurally well-known phosphates, such as (meta)autunite, torbernite, and phosphuranylite.

To achieve an immediate further improvement in the estimation of thermodynamic properties of uranyl phases and make successful predictions of the dominant uranyl phases formed during oxidative corrosion of spent fuel in underground repositories, we suggest that future experimental studies include (1) the determination of thermodynamic properties for uranyl oxide hydrates of potassium and calcium, and for uranyl silicates (e.g., sklodowskite and haiweeite), as well as the naturally abundant uranyl phosphates; and (2) structure refinements of $(UO_2)_3(PO_4)_2(H_2O)_n$ (n = 0, 4, 6), $(UO_2)_2P_2O_7$ and uranyl silicates, such as haiweeite and swamboite. Finally, calorimetric and phase-equilibrium determinations must be based on materials for which there are structure refinements and accurate chemical analyses. The proper characterization of experimental materials remains a major challenge in studies of these complex uranyl phase assemblages.

Because the molar contributions (g_i and h_i) obtained by the regression technique are average contributions of a polyhedron in selected U^{6+} phase structures, the reliability of predicted values depends on the model database. Thus, the thermodynamic data for U^{6+} phases with highly irregular structures should not be included in the model database or be predicted by these empirical methods. The predicted thermodynamic parameters are improved if the estimation is made within a group of phases that are structurally analogous.

ACKNOWLEDGMENTS

This work was supported by the Environmental Management Sciences Program of DOE (DE-FG07-97ER14816, R.C.E.). An early draft of this manuscript benefited greatly from critical reviews by R.J. Finch, P.C. Burns, F.C. Hill, and Kastriot Spahiu. The paper was much improved by reviews by J.W. Carey, J.P. Kaszuba, and W.M. Murphy.

REFERENCES CITED

Åberg, M. (1978) The crystal structure of hexaaqua-tri-μ-hydroxo-μ_3-oxo-triuranyl (VI) nitrate tetrahydrate, $[(UO_2)_3O(OH)_3(H_2O)_6]NO_3\cdot 4H_2O$. Acta Chemica Scandinavica, A32, 101–107.

Alcock, N.W., Roberts, M.M., and Brown, D. (1982) Actinide structural studies. 3. The crystal and molecular structures of $UO_2SO_4H_2SO_4\cdot 5H_2O$ and $(NpO_2SO_4)_2H_2SO_4\cdot 4H_2O$. Journal of Chemical Society Dalton Transactions, 1982, 869–873.

Allpress, J.G. (1965) The crystal structure of barium diuranate, BaU_2O_7. Journal of Inorganic and Nuclear Chemistry, 27, 1521–1527.

Alwan, A.K. and Williams, P.A. (1980) The aqueous chemistry of uranyl minerals. Part 2. Minerals of liebigite group. Mineralogical Magazine, 43, 665–667.

Appleman, D.E. and Evans, H.T. (1965) The crystal structure of synthetic anhydrous carnotite, $K_2(UO_2)_2V_2O_8$, and its cesium analogue, $Cs_2(UO_2)_2V_2O_8$. American Mineralogist, 50, 825–842.

Atencio, D., Neumann, R., Silva, A.J.G.C., and Mascarenhas, Y.P. (1991) Phurcalite from Perus, São Paulo, Brazil and redetermination of its crystal structure. Canadian Mineralogist, 29, 95–105.

Baran, V. (1992) Uranium (VI)-oxygen chemistry (uranyl hydroxo complexes, uranates, oxides). Nuclear Research Institute, Rez Czechoslovakia, 135 p.

Barner, J.O. (1985) Characterization of LWR spent fuel MCC-approved testing material-ATM-101. Richland, WA PNL-5109, Rev.1 UC-70. Richland, WA: Pacific Northwest Laboratory.

Baturin, S.V. and Sidorenko, G.A. (1985) Crystal structure of weeksite $(K_{.62}Na_{.38})(UO_2)_2[Si_5O_{13}]\cdot 3H_2O$. Doklady Akademii Nauk SSSR, 282, 1132–1136 (in Russian).

Borene, J. and Cesbron, F. (1970) Structure cristalline de l'uranyl-vanadate de nikel tétrahydraté $Ni(UO_2)_2(VO_4)_2\cdot 4H_2O$. Bulletin de la Société Francaise Minéralogie Cristallographie, 93, 426–432.

——— (1971) Structure cristalline de la curiénite $Pb(UO_2)_2(VO_4)_2\cdot 5H_2O$. Bulletin Société Francaise Minéralogie Cristallographie, 94, 8–14.

Brandenburg, N.P and Loopstra, B.O. (1973) Uranyl sulphate hydrate, $UO_2SO_4\cdot 3^1/_2H_2O$. Crystal Structure Communication, 2, 243–246.

——— (1978) β-uranyl sulphate and uranyl selenate. Acta Crystallographica, B34, 3734–3736.

Bruton, C.J. and Shaw, H.F. (1988) Geochemical simulation of reaction between spent fuel waste form and J-13 water at 25 °C and 90 °C. In M.J. Apted and R.E. Westerman, Eds., Scientific Basis for Nuclear Waste Management XI, Materials Research Society Proceedings, 112, 473–484.

Burns, P.C. (1998) The structure of boltwoodite and implications of solid solution toward boltwoodite. Canadian Mineralogist, 36, 1069–1075.

Burns, P.C., Miller, M.L., and Ewing, R.C. (1996) U^{6+} minerals and inorganic phases: A comparison and hierarchy of crystal structures. Canadian Mineralogist, 34, 845–880.

Burns, P.C., Ewing, R.C., and Miller, M.L. (1997a) Incorporation mechanisms of actinide elements into the structure of U^{6+} phases formed during the oxidation of spent nuclear fuel. Journal of Nuclear Materials, 245, 1–9.

Burns, P.C., Ewing, R.C., and Hawthorne, F.C. (1997b) The crystal chemistry of hexavalent uranium: Polyhedral geometries, bond-valence parameters and polymerization of polyhedral. Canadian Mineralogist, 35, 1551–1570.

Burns, P.C., Finch, R.J., Hawthorne, F.C., Miller, M., and Ewing, R.C. (1997c) The crystal structure of ianthinite, $[U_2^{4+}(UO_2)_4O_6(OH)_4(H_2O)_4](H_2O)_5$: a possible phase for Pu^{4+} incorporation during the oxidation of spent nuclear fuel. Journal of Nuclear Materials, 249, 199–206.

Casas, I., Bruno, J., Cera, E., Finch, R.J., and Ewing R.C (1997a) Characterization and dissolution of a becquerelite from Shinkolobwe, Zaire. Geochimica et Cosmochimica Acta, 61, 3879–3884.

Casas, I., Perez, I., Torrero, E., Bruno, J., Cera, E., and Duro, L. (1997b) Dissolution studies of synthetic soddyite and uranophane, SKB Technical Report, 97-15, 36p.

Cejka, J. and Urbanec, Z. (1990) Secondary Uranyl Minerals. Academia Czechoslovak Academy of Sciences, Prague, 93 p.

Chen, C.-H. (1975) A method of estimate Gibbs free energies of formation of silicate minerals at 298.15K. American Journal of Science, 275, 801–817.

Chermak, J.A. and Rimstidt, J.D. (1989) Estimating the thermodynamic properties (ΔG_f^0 and ΔH_f^0) of silicate minerals at 298K from the sum of polyhedral contributions. American Mineralogist, 74, 1023–1031.

Christ, C.L., Clark, J.R., and Evans, H.T. (1955) Crystal structure of rutherfordine, UO_2CO_3. Science, 121, 472–473.

Clark, S.B., Ewing, R.C., and Schaumloffel, J.C. (1998) A method to predict free energies of formation of mineral phases in the U(VI)-SiO_2-H_2O system. Journal of Alloys and Compounds, 271, 189–193.

Cremers, T.L., Eller, P.G., Larson, E.M., and Rosenzweig, A. (1986) Single-crystal structure of lead uranate (VI). Acta Crystallographica, C42, 1684–1685.

Dalley, N.K., Mueller, M.H., and Simonsen, S.H. (1971) A neutron diffraction study of uranyl nitrate dihydrate. Inorganic Chemistry, 10, 323–328.

Debets, P.C. (1966) The structure of β-UO_3. Acta Crystallographica, B24, 400–402.

Deliens, M., Piret, P., and Comblain, G. (1981) Les Minéraux secondaires d'Uranium du Zaire. Musée Royale de l'Afrique Centrale. Tervuren, 113 p.

Demartin, F., Gramaccioli, C.M., and Pilati, T. (1992) The importance of accurate crystal structure determination of uranium minerals. II. Soddyite $(UO_2)_2(SiO_4)\cdot 2H_2O$. Acta Crystallographica, C48, 1–4.

Demartin, F., Diella, V., Donzelli, S., Gramaccioli, C.M., and Pilati, T. (1991) The importance of accurate crystal structure determination of uranium minerals. I. Phosphuranylite $(KCa(H_3O)_3(UO_2)_7(PO_4)_4O_4\cdot 8H_2O$. Acta Crystallographica, B47, 439–446.

Dickens, P.G., Stuttard, G.P., Ball, R.G.J., Powell, A.V., Hull, S., and Patat, S. (1992) Powder neutron diffraction study of the mixed uranium vanadium oxides $Ce_2(UO_2)_3(V_2O_8)$ and UVO_5. Journal of Material Chemistry, 2, 161–166.

Evans, H.T. Jr. (1963) Uranyl ion coordination. Science, 141, 154–157.

Finch, R.J. (1994) Paragenesis and crystal chemistry of the uranyl oxide hydrates. Ph.D. thesis, 261 p. University of New Mexico.

——— (1997) Thermodynamic stabilities of U(VI) minerals: Estimated and observed relationships. In W.J. Gray and I.R. Triay , Eds., Scientific Basis for Nuclear Waste Management XX, Materials Research Society Proceedings, 465, 1185–1192.

Finch R.J., Cooper, M.A., Hawthorne, H.C., and Ewing, R.C. (1996) The crystal structure of schoepite, $[(UO_2)_8O_2(OH)_{12}](H_2O)_{12}$. Canadian Mineralogist, 34, 1071–1088.

Finch, R.J. and Ewing, R.C. (1991) Alteration of natural UO_2 under oxidizing conditions from Shinkolobwe, Katanga, Zaire: A natural analogue for the corrosion of spent fuel. Radiochimica Acta, 52/53, 395–401.

——— (1992) The corrosion of uraninite under oxidizing conditions. Journal of Nuclear Materials, 190, 133–156.

Fitch, A.N. and Cole, M. (1991) The structure of $KUO_2PO_4\cdot 3D_2O$ refined from neutron and synchrotron radiation powder diffraction data. Materials Research Bulletin, 26, 407– 414.

Freeze, R.A. and Cherry, A.J. (1979) Groundwater, p. 254–289. Prentice-Hall, Inc. Englewood Cliffs, New Jersey.

Frondel, C. (1958) Systematic Mineralogy of Uranium and Thorium. U.S. Geological Survey Bulletin 1064, Washington, D.C., U.S. Government Printing Office, 400 p.

Garrels, R.M. and Christ, C.L. (1959) Behavior of uranium minerals during oxidation. U.S. Geological Survey Professional Paper, 320 (part 1), 2–13.

Garrels, R.M. and Weeks, A.D. (1959) Geological setting of the Colorado Plateau ores. U.S. Geological Survey Professional Paper, 320 (part 6), 81–90.

Gasperin, M. (1987a) Synthèse et structure du diborouranate de cesium: $CsNbUO_6$. Acta Crystallographica, C43, 404–406.

———(1987b) Synthèse et structure du diborouranate de calcium. $CaB_2U_2O_{10}$. Acta Crystallographica, C43, 1247–1250.

——— (1987c) Synthèse et structure du diborouranate de magnésium. MgB_2UO_7. Acta Crystallographica, C43, 2264–2266.

——— (1988) Synthèse et structure du borouranate de sodium, $NaBUO_5$. Acta Crystallographica, C44, 415–416.

——— (1990) Synthèse et structure du borouranate de lithium, $LiBUO_5$. Acta Crystallographica, C46, 372–374.

Gebert, E., Hoekstra, H.R., Reis, A.H., and Peterson, S.W. (1978) The crystal structure of lithium uranate. Journal of Inorganic and Nuclear Chemistry, 40, 65–68.

Ginderow, D. (1988) Structure de l'uranophane alpha, $Ca(UO_2)_2(SiO_3OH)_2\cdot 5H_2O$. Acta Crystallographica, C44, 421–424.

Grenthe, I., Fuger, J, Konings, R.J.M, Lemire, R.J., Muller, A.B., Nguyen-Trung, C., and Wanner, H. (1992) Chemical Thermodynamics of Uranium, 713 p. North-Holland, Amsterdam.

Hanic, F. (1960) The crystal structure of meta-zeunerite $Cu(UO_2)_2(AsO_4)_2\cdot 8H_2O$. Czechoslovak Journal of Physics, 10, 169–181.

Hazen, R.M. (1985) Comparative crystal chemistry and the polyhedral approach. In Mineralogical Society of America Reviews in Mineralogy, 14, 317–345.

——— (1988) A useful fiction: Polyhedral modelling of mineral properties. American Journal of Science, 288-A, 242–269.

Hemingway, B.S. (1982) Thermodynamic properties of selected uranium compounds and aqueous species at 298.15K and 1 bar and at higher temperatures-preliminary model for the origin of coffinite deposits. U.S. Geological survey open-file report 82, 619, 90 p.

Hemingway, B.S., Haas, J.L. Jr., and Robinson, G.R. Jr. (1982) Thermodynamic properties of selected minerals in the system Al_2O_3-CaO-SiO_2-H_2O at 298.15K and 1 bar pressure and at high temperatures. U.S. Geological Survey Bulletin 1544, 70 p.

Hoekstra, H.R. and Siegel, S. (1973) The uranium trioxide-water system. Journal of Inorganic and Nuclear Chemistry, 35, 761–779.

Johnson, L.H. and Shoesmith, D.W. (1988) Spent fuel. In W. Lutze and R.C. Ewing, Eds. Radioactive Waste Forms for the Future, p. 635–698. North-Holland, Amsterdam.

Johnson, L.H. and Werme, L.O. (1994) Materials characteristics and dissolution behavior of spent nuclear fuel. Materials Research Society (MRS) Bulletin, 19(2), 24–27.

Karpov, I.K. and Kashik, S.A. (1968) Computer calculation of standard isobaric-isothermal potentials of silicates by multiple regression from a crystallochemical classification. Geochemistry International, 5, 706–713.

Khosrawan-Sazedj, F. (1982a) The crystal structure of meta-uranocircite II. $Ba(UO_2)_2(PO_4)_2 \cdot 6H_2O$. Tschermaks Mineralogische und Petrographische Mitteilungen, 29, 193–204.

——— (1982b) On the space group of threadgoldite. Tschermaks Mineralogische und Petrographische Mitteilungen, 30, 111–115.

Kovba, L.M. (1971) The crystal structure of potassium and sodium monouranates. Radiokhimiya, 13, 309–331 (in Russia).

——— (1972) Crystal structure of $K_2U_7O_{22}$. Journal of Structural Chemistry, 13, 235–238.

Kovba, L.M., Ippolitova, E.A., Simanov, Yu. P., and Spitsyn, V.I. (1958) The X-ray investigation of uranates of alkali elements. Doklady Akademii Nauk SSSR, 242, 1083–1085 (in Russian).

Langmuir, D. (1978) Uranium solution-mineral equilibria at low temperatures with applications to sedimentary ore deposits. Geochimica et Cosmochimica Acta, 42, 547–569.

Lee, M.R. and Jaulmes, S. (1987) Novelle série d'oxydes dérivés de la structure de α-U_3O_8: $M(II)UMo_4O_{16}$. Journal of Solid State Chemistry, 67, 364–368.

Linde, S.A., Gorbunova, Y.E., Lavrov, A.V., and Kuznetsov, V.G. (1978) Synthesis and structure of $CsUO_2(PO_3)_3$ crystals. Doklady Akademii Nauk SSSR, 242, 1083–1085 (in Russian).

Linde, S.A., Gorbunova, Y.E., and Lavrov, A.V. (1980) Crystal structure of $K_4UO_2(PO_4)_2$. Zhurnal Neoganicheskoi Khimii, 25, 1992–1994 (in Russian).

Linde, S.A., Gorbunova, Y.E., Lavrov, A.V., and Pobedina, A.B. (1984) The synthesis and structure of crystals of sodium uranyl pyrophosphate $Na_2UO_2P_2O_7$. Zhurnal Neoganicheskoi Khimii, 29, 1533–1537 (in Russian).

Loopstra, B.O. and Cordfunke, E.H.P. (1966) On the structure of α-UO_3. Recueil des Travaux Chimiques des Pay-Bas et de la Belgique RTCPA, 85, 135–142.

Loopstra, B.O. and Rietveld, H.M. (1969) The structure of some alkaline-earth metal uranates. Acta Crystallographica, B25, 787–791.

Loopstra, B.O., Taylor, J.C., and Waugh, A.B. (1977) Neutron powder profile studies of the gamma uranium trioxide phases. Journal of Solid State Chemistry, 20, 9–19.

Makarov, Y.S. and Anikina, L.I. (1963) Crystal structure of umohoite $(UMoO_6(H_2O)_2) \cdot 2H_2O$. Geochemistry, 14–21.

Makarov, Y.S. and Ivanov, V.I. (1960) The crystal structure of meta-autunite, $Ca(UO_2)_2(PO_4)_2 \cdot 6H_2O$. Doklady Academy of Sciences SSSR, Earth Science Section, 132, 601–603.

Mattigod, S.V. and Sposito, G. (1978) Improved method for estimating the standard free energy of formation ($\Delta G^0_{f,298.15}$) of smectites. Geochimica et Cosmochimica Acta, 42, 1753–1762.

Mayer, H. and Mereiter, K. (1986) Synthetic bayleyite, $Mg_2[UO_2(CO_3)_3] \cdot 18H_2O$: thermochemistry, crystallography and crystal structure. Tschermaks Mineralogische und Petrographische Mitteilungen, 35, 133–146.

McKelvey, V.E., Everhart, D.L., and Garrels, R.M. (1955) Origin of uranium deposits. Economic Geology (50th Anniversary Volume), 464–533.

Mereiter, K. (1982) The crystal structure of liebigite, $Ca_2UO_2(CO_3)_3 \cdot \approx 11H_2O$. Tschermaks Mineralogische und Petrographische Mitteilungen, 30, 129–139.

——— (1986a) Synthetic swartzite, $CaMg[UO_2(CO_3)_3] \cdot 12H_2O$ and its strontium analogue, $SrMg[UO_2(CO_3)_3] \cdot 12H_2O$: crystallography and crystal structure. Neues Jahrbuch für Mineralogie-Monatshefte, 1986, 481–492.

——— (1986b) Neue kristallographische Daten ueber das Uranmineral Andersonit. Anzeiger der Oesterreichischen Akademie der Wissenschaften, Mathematisch-Naturwissenschaftliche Klasse OSAWA, 3, 39–41.

——— (1986c) Structure of strontium tricarbonato-dioxouranate(VI) octahydrate. Acta Crystallographica, C42, 1678–1681.

——— (1986d) Crystal structure refinements of two francevillites, (Ba,Pb) $[(UO_2)_2V_2O_8] \cdot 5H_2O$. Neues Jahrbuch für Mineralogie-Monatshefte, 1986, 552–560.

Mereiter, K. (1988) Structure of caesium tricarbonato-dioxouranate(VI) hexahydrate. Acta Crystallographica, C44, 1175–1178.

Miller, S.A., and Taylor, J.C. (1986) The crystal structure of saleeite, $Mg[UO_2PO_4]_2 \cdot 10H_2O$. Zeitschrift für Kristallographie, 177, 247–253.

Moll, H., Geipel, G., Matz, W., Bernhard, G., and Nitsche, H. (1996) Solubility and speciation of $(UO_2)SiO_4 \cdot 2H_2O$ in aqueous system. Radiochimica Acta, 74, 3–7.

Morosin, B. (1978) Hydrogen uranyl tetrahydrate, a hydrogen ion solid electrolyte. Acta Crystallographica, B34, 3732–3734.

Murphy, W.M. and Pabalan, R.T. (1995) Review of empirical thermodynamic data for uranyl silicate minerals and experimental plan. Center for Nuclear Waste Regulation Analyses, San Antonio, Texas, CNWRA 95-014, 43 p.

Nguyen, S.N., Silva, R.J., Weed, H.C., and Andrews J.E. Jr. (1992) Standard Gibbs free energies of formation at temperature 303.15K of four uranyl silicates: soddyite, uranophane, sodium boltwoodite, and sodium weeksite. Journal of Chemical Thermodynamics, 24, 259–276.

Niinisto, L., Toivonen, R.T., and Valkonen, J. (1979) Uranyl (VI) compounds. II. The crystal structure of potassium uranyl sulfate dihydrate, $K_2UO_2(SO_4)_2 \cdot 2H_2O$. Acta Chemica Scandinavica, A33, 621–624.

Nriagu, J.O. (1975) Thermodynamical approximations for clay minerals. American Mineralogist, 60, 834–839.

Oversby, V.M. (1994) Nuclear waste materials. In B.R.T. Frost, Eds., Nuclear Materials, Vol. 10B, Material Science and Technology, A comprehensive treatment, VCH, Weinheim, Germany, 392–442.

Pagoaga, M.K., Appleman, D.E., and Stewart, J.M. (1987) Crystal structure and crystal chemistry of the uranyl oxide hydrates becquerelite, billietite, and protasite. American Mineralogist, 72, 1230–1238.

Pearcy, E.C., Prikryl, J.D., Murphy, W.M., and Leslie, B.W. (1994) Alteration of uraninite from the Nopal I deposit, Peña Blanca district, Chihuahua, Mexico, compared to degradation of spent nuclear fuel in the proposed U.S. high-level nuclear waste repository at Yucca Mountain, Nevada. Applied Geochemistry, 9, 713–732.

Perrin, A. (1976) Structure cristalline du nitrate de dihydroxo diuranyle tetrahydrate. Acta Crystallographica, B32, 1658–1661.

Piret, P. (1985) Structure crystalline de la fourmarierite, $Pb(UO_2)_4O_3(OH)_4 \cdot 4H_2O$. Bulletin de Minéralogie, 108, 659–665.

Piret, P. and Declercq, J.P. (1983) Structure crystalline de l'upalite $Al[(UO_2)_3O(OH)(PO_4)_2] \cdot 7H_2O$: Un example de macle mimétique. Bulletin de Minéralogie, 106, 383–389.

Piret, P. and Deliens, M. (1987) Les phosphates d'uranyle et d'aluminium de Kobokobo. IX. L'althupite $AlTh(UO_2)[(UO_2)_3O(OH)(PO_4)_2]_2(OH)_3 \cdot 15H_2O$. Nouveau minéral propriétés et structure cristalline. Bulletin de Minéralogie, 110, 443–449.

Piret, P. and Wauters-Stoop, D. (1980) Structure cristalline de la sengiérite. Bulletin de Minéralogie, 103, 176–178.

Piret, P., Piret-Meunier, J., and Declercq, J.-P. (1979) Structure of phuralumite. Acta Crystallographica, B35, 1880–1882.

Piret, P., Deliens, M. Piret-Meunier, J., and Germain, G. (1983) La sayrite, $Pb_2[(UO_2)_2O_6(OH)_2] \cdot 4H_2O$: Nouveau minéral propriétés et structure cristalline. Bulletin de Minéralogie, 106, 299–304.

Reis, A.H. Jr., Hoekstra, H.R., Gebert, E., and Peterson, S.W. (1976) Redetermination of the crystal structure of barium uranate. Journal of Inorganic and Nuclear Chemistry, 38,1481–1485.

Reshetov, K.V. and Kovba, L.M. (1966) Structures of $SrUO_{(4-x)}$, $CdUO_{(4-x)}$, and Li_4UO_5. Journal of Structural Chemistry, 7, 589–590.

Rosenzweig, A. and Ryan, R.R. (1975) Refinement of the crystal structure of cuprosklodowskite, $Cu[(UO_2)_2(SiO_3OH)_2] \cdot 6H_2O$. American Mineralogist, 60, 448–453.

——— (1977) Kasolite, $Pb(UO_2)(SiO_4) \cdot H_2O$. Crystal Structure Communication, 6, 617–621.

Ross, M. and Evans, H.T. Jr. (1960) The crystal structure of cesium biuranyl trisulfate, $Cs_2(UO_2)_2(SO_4)_3$. Journal of Inorganic and Nuclear Chemistry, 15, 338–351.

——— (1964) Study of torbernite minerals. I. The crystal structure of abernathyite and the structurally related compounds $NH_4(UO_2AsO_4) \cdot 3H_2O$ and $K(H_3O)(UO_2AsO_4) \cdot 6H_2O$. American Mineralogist, 49, 1578–1602.

Ryan, R.R. and Rosenzweig, A. (1977) Sklodowskite, $MgO \cdot 2UO_3 \cdot 2SiO_2 \cdot 7H_2O$. Crystal Structure Communication, 6, 611–615.

Saine, M.C. (1989) Synthèse et structure de $K_2[(UO_2)_2O_3]$ monoclinique. Journal of Less-Common Metals, 154, 361–365.

Sandino, M.C.A. and Grambow, B. (1994) Solubility equilibria in the U(VI)-Ca-K-Cl-H_2O system: Transformation of schoepite into becquerelite and compreignacite. Radiochimica Acta, 66/67, 37–43.

Serezhkin, V.A., Chuvaev, V.F., Kovba, L.M., and Trunov, V.K. (1973) The structure of synthetic iriginite. Doklady Akademii Nauk SSSR, 210, 873–876 (in Russian).

Serezhkin, V.A., Efremov, V.A., and Trunov, V.K. (1980) The crystal structure of α-$UO_2MoO_4 \cdot 2H_2O$. Kristallografiya, 25, 861–865 (in Russian).

Serezhkin, V.A., Soldatkina, M.A., and Efremov, V.A. (1981) Crystal structure of $MgUO_2(SO_4)_2 \cdot 11H_2O$. Journal of Structural Chemistry, 22, 454–457.

Shoemaker, E.M. (1956) Occurrence of uranium in diatremes on the Navajo and Hopi Reservations, Arizona, New Mexico, and Utah. U.S. Geological Survey Professional Paper 300, 179–185.

Shoesmith, D.W. and Sunder, S. (1992) The prediction of nuclear-fuel (UO_2) dissolution rates under waste-disposal conditions. Journal of Nuclear Materials, 190, 20–35.

Siegel, S., Hoekstra, H.R., and Gebert, E. (1972) The structure of γ-uranyl hydroxide, $UO_2(OH)_2$. Acta Crystallographica, B28, 3469–3473.

Smith, D.K. (1984) Uranium mineralogy. In. F. Ippolito, B. DeVero, and G. Capaldi, Eds., Uranium Geochemistry, Mineralogy, Geology Exploration and Resources. 43–88. Institute of Mining and Metallurgy, London.

Sposito, G. (1986) The polymer model of thermodynamical clay mineral stability. Clays and Clay minerals, 34, 198–203.

Stergiou A.C., Rentzeperis, P.J., and Sklavounos, S. (1993) Refinement of crystal structure of metatorbernite. Zeitschrift für Kristallographie, 205, 1–7.

Stohl, F.V. and Smith, D.K. (1981) The crystal chemistry of the uranyl silicate minerals. American Mineralogist, 66, 610–625.

Sunder, S., Shoesmith, D.W., Kolar, M., and Leneveu, D.M. (1998) From laboratory experiments to geological disposal vault: Calculation of used nuclear fuel dissolution rates. In I.G. McKinley and C. McCombie, Eds., Scientific Basis for Nuclear Waste Management XXI, Materials Research Society Proceedings, 506, 273–280.

Tabachenko, V.V., Kovba L.M., and Serezhkin, V.N. (1983) Crystal structures of molybdatouranylates of magnesium and zinc of composition $M(UO_2)_3(MoO_4)_4 \cdot (H_2O)_8$ (m=Mg, Zn). Koordinatsionnaya Khimiya, 9, 1568–1571 (in Russian).

Tabachenko, V.V., Balashov, V.L., Kovba L.M., and Serezhkin, V.N. (1984a) Crystal structures of barium uranyl molybdate $Ba(UO_2)_3(MoO_4)_4 \cdot 4H_2O$. Koordinatsionnaya Khimiya, 10, 854–857 (in Russian).

Tabachenko, V.V., Kovba L.M., and Serezhkin, V.N. (1984b) Crystal structures of $Mg(UO_2)_6(MoO_4)_7 \cdot 18H_2O$ and $Sr(UO_2)_6(MoO_4)_7 \cdot 15H_2O$. Koordinatsionnaya Khimiya, 9, 558–562 (in Russian).

Tardy, Y. and Garrels, R.M. (1974) A method of estimating the Gibbs free energies of formation of layer silicates. Geochimica et Cosmochimica Acta, 38, 1101–1116.

—— (1976) Prediction of Gibbs free energies of formation- I. Relationships among Gibbs free energies of formation of hydroxides, oxides and aqueous ions. Geochimica et Cosmochimica Acta, 40, 1051–1056.

—— (1977) Prediction of Gibbs free energies of formation- II. Monovalent and divalent metal silicates. Geochimica et Cosmochimica Acta, 41, 87–92.

Taylor, J.C. (1971) The structure of α-form uranyl hydroxide. Acta Crystallographica, B27, 1088–1091.

Taylor, J.C. and Bannister, M.J. (1972) A neutron diffraction study of the anisotropic thermal expansion of β-uranyl dihidroxide. Acta Crystallographica, B28, 2995–2999.

Taylor, J.C. and Mueller, M.H. (1965) A neutron diffraction study of uranyl nitrate hexahydrate. Acta Crystallographica, 19, 536–543.

Taylor, J.C., Stuart, W.I., and Mumme, I.A. (1981) The crystal structure of curite. Journal of Inorganic and Nuclear Chemistry, 43, 2419–2423.

Van Der Putten, N. and Loopstra, B.O. (1974) Uranyl sulphate, $UO_2SO_4 \cdot 2^1/_2H_2O$. Crystal Structure Communication, 3, 377–380.

Van Egmond, A.B. (1976) Investigations on cesium uranates, V. The crystal structure of Cs_2UO_4, $Cs_4U_5O_{17}$, $Cs_2U_7O_{22}$, and $Cs_2U_{15}O_{46}$. Journal of Inorganic and Nuclear Chemistry, 38, 1649–1651.

Van Egmond, A.B. and Cordfunke, E.H.P. (1976) Investigation on potassium and rubidium uranates. Journal of Inorganic and Nuclear Chemistry, 38, 2245–2247.

Van Genderen, L.C.G. and Van Der Weijden, C.H. (1984) Prediction of Gibbs free energies of formation and stability constants of some secondary uranium minerals containing the uranyl group. Uranium, 1, 249–256.

Vieillard, P. and Tardy, Y. (1988) Estimation on enthalpies of formation of minerals based on their refined crystal structures. American Journal of Science, 288, 997–1040.

Viswanathan, K. and Harneit, O. (1986) Refined crystal structure of β-uranophane $Ca(UO_2)_2(SiO_3OH) \cdot 5HO$. American Mineralogist, 71, 1489–1493.

Vochten, E.M. and Van Haverbeke, L. (1990) Transformation of schoepite into the uranyl oxide hydrates: becquerelite, billietite and wolsendorfite. Mineralogy and Petrology, 43, 65–72.

Vochten, R., Van Haverbeke, L., Van Springei, K., Blaton, N., and Peeters, O.M. (1995) The structure and physicochemical characteristic of synthetic zippeite. Canadian Mineralogist, 33, 1091–1101.

Weeks, A.D. and Thompson, M.E. (1954) Identification and occurrence of uranium and vanadium minerals from the Colorado Plateau: U.S. Geological Survey Bulletin, 1009–B, 13–62.

Wilson, C.N. (1988) Summary of results from the series 2 and series 3 NNWAI bare fuel dissolution test. In M.J. Apted and R.E. Westerman, Eds., Scientific Basis for Nuclear Waste Management XX, Materials Research Society Proceeding, 112, 473–484.

Wolf, R. and Hoppe, R. (1986) Neues über Oxouranate(VI): Na_4UO_5 und K_4UO_5. Revue de Chimie Minérale, 23, 828–848.

Wronkiewicz, D.J., Bates, J.K., Gerding, T.J., and Veleckis, E. (1992) Uranium release and secondary phase formation during unsaturated testing of UO_2 at 90 °C. Journal of Nuclear Materials, 190, 107–127.

Zachariasen, W.H. (1954) Crystal structure studies of the 5f-series of elements. XXI. The crystal structure of magnesium orthouranate. Acta Crystallographica, 7, 788–791.

Zalkin, A., Templeton, L.K., and Templeton, D.H. (1989) Structure of rubidium uranyl(VI) trinitrate. Acta Crystallographica, C45, 810–811.

MANUSCRIPT RECEIVED APRIL 20, 1998
MANUSCRIPT ACCEPTED NOVEMBER 11, 1998
PAPER HANDLED BY J. WILLIAM CAREY

APPENDIX 1. A DISCUSSION ON THE SOLUBILITY DATA OF URANYL SILICATES

Nguyen et al. (1992) completed solubility measurements at 30 °C on soddyite $(UO_2)_2SiO_4 \cdot 2H_2O$, uranophane $Ca(H_3O)_2(UO_2)_2(SiO_4)_2 \cdot 3H_2O$, sodium boltwoodite $Na(H_3O)(UO_2)SiO_4 \cdot H_2O$, and sodium weeksite $Na_2(UO_2)_2(Si_2O_5)_3 \cdot 4H_2O$ (the number of "H_2O" is 7 instead of 4 in the formula for sodium weeksite as given in the abstract of the original paper, but the authors used the correct number in Table 1 and the dissolution equation, Eq.1). The uranyl silicate samples used in the experiments were synthesized and characterized by X-ray powder diffraction (XRD), Fourier transform infrared spectroscopy (FTIR), and chemical analysis. The standard Gibbs free energies calculated by the authors based on their solubility data are –3658.0 ± 4.8 kJ/mol, –6210.6 ± 7.6 kJ/mol, –2966.0 ± 3.6 kJ/mol, and –9088.5 ± 18.4 kJ/mol for soddyite, uranophane, sodium boltwoodite, and sodium weeksite, respectively. However, according to the structure refinements of these phases, the formula of uranophane is $Ca[(UO_2)(SiO_3OH)]_2 \cdot 5H_2O$ (Ginderow 1988); weeksite has a formula of $K_2[(UO_2)_2(Si_5O_{13})] \cdot 3H_2O$ (Baturin and Sidorenko 1985), with the Si:U molar ratio in the formula of weeksite being 2.5:1 instead of 3:1. Stohl and Smith (1981) have suggested a formula of $K(H_3O)[(UO)_2(SiO_4)]$ for boltwoodite based on a structural determination, but the most recent refinement of the crystal structure of a boltwoodite solid solution indicates that there is no "H_3O" in the structure, and the sheet in boltwoodite is similar to that of uranophane with the number of molecular waters in the interlayer being approximately 1.5 (Burns 1998). Thus, a formula of $(Na,K)[(UO)_2(SiO_3OH)] \cdot 1.5H_2O$ is suggested for boltwoodite solid solution (Burns 1998). Variations in the number of water molecules in the formulas have little influence on the calculated solubility products from the solubility data if the activity of water in the aqueous solution is close to unity, but may have a more significant influence on the calculated ΔG^0_f. Thus, mineral formulas based on structural refinements, when available, are used, and the thermodynamic data have been recalculated using the formulas based on structure refinements.

Although identified on the basis of XRD patterns and FTIR spectra, the chemical analysis of the synthesized samples by Nguyen et al. (1992) are not exactly identical to their nominal stoichiometries. Synthetic soddyite was determined to have an U/Si molar ratio of 1.00:0.55 instead of 1.00:0.50, as indicated by its nominal formula. The excess silica in the soddyite sample is consistent with amorphous silica contamination, as indicated by the FTIR spectra. The measured concentrations of uranium and silicon agree well with the nominal stoichiometric values for uranophane, but calcium is lower than the theoretical value. The analyzed chemical composition of sodium boltwoodite corresponds to its theoretical value, but with a weak depletion of sodium. Although the analyzed U/Na molar ratio for the synthetic sodium weeksite is identical to the nominal stoichiometric value, the measured silica content is a little high with U/Si (molar ratio) = 0.38 rather than 0.40. The measured elemental ratios in the final solutions of the solubility experiments indicate incongruent release of elements in all the experiments. The low release of Si relative to U in the soddyite and uranophane experiments could be due to the precipitation of silica, which is partly confirmed by the high silica concentration in the solution (higher than the solubility of amorphous silica). The large excess of Na in solutions of the sodium boltwooodite and sodium weeksite experiments were mostly from the automatic NaOH titration device used for pH control, but the significantly elevated

Si/U in these solutions could have resulted from precipitation of soddyite or other minerals with low Si/U ratios. Secondary phase precipitation in the solubility experiments of sodium boltwoodite and sodium weeksite is suggested by the fluctuation of uranium solution concentrations with time, and precipitation of soddyite as a secondary mineral in the sodium boltwoodite experiment was confirmed by XRD analysis.

Murphy and Pabalan (1995) have concluded that the solubility data reported by Nguyen et al. (1992) for soddyite must be regarded as a lower limit, as equilibrium was approached only from undersaturation and that the solubility data for uranophane, sodium boltwoodite, and sodium weeksite are unreliable due to their non-nominal stoichiometric solid phase composition and incongruent elemental release in the dissolution experiments. Because soddyite precipitated in the sodium boltwoodite experiment, we have calculated a solubility product at infinite dilution (log K_{SP}) of 7.81 for soddyite using the solubility data from this experiment, which is approximately 2 log units higher than that (5.74) calculated based on the soddyite solubility experiment. This value of 7.81 represents the upper solubility limit of soddyite. Assuming that the depleted Ca and Na in the synthesized uranophane and sodium boltwoodite were replaced by hydrogen to maintain charge balance in the structure, we calculated log K_{SP} values of 8.26 and 5.6 for the analytical stoichiometric uranophane and sodium boltwoodite, respectively. In comparison with the 9.46 and 5.82 values calculated assuming the nominal stoichiometry for these two minerals, this indicates that the small compositional deviations of these minerals from their nominal stoichiometries does not significantly affect the ΔG_f^0 obtained from the solubility data. The incongruent elemental release in the solubility experiments probably resulted from dissolution of trace amounts of impurities and subsequent precipitation of secondary phases. Thus, we consider the solubility data for soddyite, uranophane, sodium boltwoodite, and sodium weeksite reported by Nguyen et al. (1992) to be plausible approximations of their solubilities.

This analysis has in part been confirmed by the dissolution experiments of soddyite and uranophane conducted by Moll et al. (1996) and Casas et al. (1997b). Moll et al. (1996) determined the solubility of soddyite at 25 °C in air and in an N_2-atmosphere beginning from undersaturation conditions. The solubility-product (log K_{SP}) obtained was 6.03 ± 0.45 in N_2 and 6.15 ± 0.53 in air. Ten solubility experiments of soddyite were conducted by Casas et al. (1997b) in solutions with different HCO_3^- concentrations (1.0 m*M* to 20 m*M*), and the calculated log K_{SP} decreases systematically as the total concentration of HCO_3^- increases. The log K_{SP} values obtained at bicarbonate concentrations between 5.0 mM to 20 m*M* were selected and averaged by Casas et al. (1997b) to obtain a log K_{SP} of 3.9 ± 0.7 for soddyite, based on the argument that other uranyl complexes play an important role in solutions with low carbonate concentrations. Because all the uranyl hydroxide and carbonate complexes were taken into account in their calculations (Cera 1998, personal communication) and no other uranyl complexes are known that may be important in the carbonate solution, this argument is questionable. Considering that: (1) the equilibria were approached from undersaturation; (2) the extrapolation of the experimental results to infinite dilution is more accurate when the ionic strength is low, we propose that the log K_{SP} values at low bicarbonate concentrations should be closer to the solubility product of soddyite. Thus, the log K_{SP} values obtained at bicarbonate concentrations between 1.0 m*M* to 2.0 m*M* were averaged to obtain a value of 5.93 ± 0.5. This value and those reported by Nguyen et al. (1992) and Moll et al. (1996) were selected and averaged to obtain a value of 5.96 $\pm$ 0.5 as the solubility product of soddyite used in this study. The log K_{SP} values for uranophane based on the 12 experiments reported by Casas et al. (1997b) are in the range of 10.75 to 12.94, with an average of $11.7 \pm .0.6$. This value is used as the solubility product of uranophane and is in fair agreement with the value of 9.42 reported by Nguyen et al. (1992).

Using the experimental results discussed above and the database of Grenthe et al. (1992), $\Delta G^0_{f,298}$ values of -3653.0 $\pm$ 2.9 kJ/mol, -6192.3 $\pm$ 3.4 kJ/mol, –2844.8 $\pm$ 3.9 kJ/mol, and –7993.9 $\pm$ 9.8 kJ/mol were obtained for soddyite, uranophane, sodium boltwoodite, and sodium weeksite, respectively.